Dyes and Pigments 176 (2020) 108180

Contents lists available at ScienceDirect

Dyes and Pigments

journal homepage: http://www.elsevier.com/locate/dyepig

The potential of anthocyanins from blueberries as a natural dye for cotton: A combined experimental and theoretical study

Kim Phan [a], Elias Van Den Broeck [b], Veronique Van Speybroeck [b], Karen De Clerck [c], Katleen Raes [d], Steven De Meester [a,*]

[a] Laboratory for Circular Process Engineering (LCPE), Department of Green Chemistry and Technology, Ghent University Campus Kortrijk, Graaf Karel de Goedelaan 5, B-8500, Kortrijk, Belgium
[b] Center for Molecular Modeling, Ghent University, Technologiepark 46, B-9052, Zwijnaarde, Belgium
[c] Department of Materials, Textiles and Chemical Engineering (MaTCh), Ghent University, Technologiepark 70A, B-9052, Zwijnaarde, Belgium
[d] Laboratory of Food Microbiology and Biotechnology, Department of Food Technology, Safety and Health, Ghent University Campus Kortrijk, Graaf Karel de Goedelaan 5, B-8500, Kortrijk, Belgium

ARTICLE INFO

Keywords:
Anthocyanins
Cotton
Density functional theory (DFT)
Molecular dynamics
Natural dye

ABSTRACT

Natural dyes might be more environmentally sustainable compared to their synthetic counterparts, however in general their performance is worse. Therefore, typically metallic mordants are applied to improve the natural dye's affinity towards substrates, but this is not a suitable technique in a 'green story'. In this paper, we test the potential of using anthocyanins from blueberry waste for dyeing cotton with biomordants, which are selected to tailor the intermolecular interactions such as hydrogen bonds, ionic bonds and π-π interactions with the dye molecule. In the experimental part, parameters during extraction and dyeing were optimized (e.g. temperature, pH, dyeing time and concentration). The effect of the (bio)mordants was monitored by Fourier transform infrared spectroscopy, spectrophotometric measurements and standard ISO wash and light tests. It was shown that stannous chloride stands out as metallic mordant, while no biomordants show sufficient intermolecular interactions to replace this metal salt. The experimental study has been corroborated with a series of molecular modeling calculations to obtain more insight into the intermolecular interactions between dye and (bio)mordants. To this end, both static Density Functional Theory based calculations as semi-empirical and force field based molecular dynamics calculations have been performed. The results indeed confirm that, in general, too small interaction energies for the biomordants of interest with the dye molecules are found, in correspondence with experimental findings. Overall, by performing systematic experiments in combination with the interpretation of the molecular models, this study yields valuable insights into the development of green routes towards use of anthocyanins as a natural dye for cellulose-based materials.

1. Introduction

Since mid 19th century, the discovery of the synthetic dye 'mauve' induced an avalanche of research within synthetic chemistry, and along with industrialization, synthetic dyes became the standard in many applications such as cosmetics, textiles and food colorants, pushing natural dyes towards the background. Even though these dyes are often cheap, produce a variety of colors, possess good fastness values, some disadvantages are sometimes connected as well such as allergic, toxic and even carcinogenic properties, which are harmful for humans and the environment [1]. The increased awareness for eco-friendliness and sustainability is shifting the momentum back to natural dyes [2]. From economic and environmental point of view, waste streams or by-products generated from food processing industries contain high-added value compounds including natural dyes, so there is sustainable feedstock available on the market at relatively low cost [3]. For instance, approximately 20% of the raw blueberries remain as pomace during juice processing [4]. However, natural dyes have some shortcomings in terms of stability and affinity for substrates. Therefore, they require dye procedures or fixatives such as mordants [5]. Most of the time, these mordants are metal salts, which could form coordination complexes with the natural dye molecule. This improves the stability,

* Corresponding author.
E-mail address: Steven.DeMeester@UGent.be (S. De Meester).

https://doi.org/10.1016/j.dyepig.2019.108180
Received 26 September 2019; Received in revised form 12 December 2019; Accepted 30 December 2019
Available online 3 January 2020

but (heavy) metallic mordants also come along with potential pollution and waste water issues [5]. Biomordants, often tannin rich compounds, which are responsible for the formation of hydrogen bonds, might be able to substitute these metallic equivalents as they fit better in a shift towards sustainability [6].

This paper focuses on anthocyanins, which is a subclass within the class of flavonoids and, which are responsible for red till bluish colors in most flowers, higher plants, fruit and vegetables. Anthocyanins consist of a typical C6–C3–C6 aglycon, which is often glycosylated. Within plants, these sugar moieties are acylated. The most frequently occurring anthocyanidins are cyanidin, delphinidin, malvidin, pelargonidin, peonidin and petunidin. Anthocyanins are very prone to pH-fluctuations. At different pH-values it could undergo reversible reactions as illustrated in Fig. S1. Between pH 1 till 3 the anthocyanins exist as the red flavylium cation (A). Furthermore, anthocyanins are known to have three major sites of deprotonation [7]. When the flavylium cation loses its first acidic proton (C_5, C_7 or $C_{4'}$) around pH 5, this yields the quinoidal base (B) (kinetic product). These quinoidal bases could undergo subsequent deprotonations around neutrality and pH 8.5 to form the anionic (B^-) and dianionic quinoidal bases (B^{2-}), respectively [7]. A second pathway yields the colorless hemiketal isomer (thermodynamic product, C), which occurs when a water molecule performs a nucleophilic attack at the C_2 position of the flavylium cation. Thereafter, a tautomerization reaction, with ring opening, results into the light-yellow cis-chalcone (D), which can possibly isomerize to trans-chalcone (E) [8–11].

Anthocyanins are mostly applied as food colorant [12], but also have potential to find their way into non-food applications (e.g. textile substrates and dye sensitized solar cells). Cotton [13–18], leather [15], wool [13,19–22], silk [14,15,18,23–25] and human hair [26] were dyed with several by-products such as fruit and vegetable pressed and liquid residues [22]. Examples are: blackcurrant fruit waste [18,21,26], sunflower seed [19], red cabbage extract [20], onion outer skins [23], grape pomace [13], purple sweet potato [15,25], black cowpea seed coat [14] and mulberry fruits [16,17,24]. Several approaches to improve the affinity of anthocyanins were already tested. However, in general four mechanisms are distinguished to improve the affinity of anthocyanins on textile fibers: (i) metal salts, (ii) biomordants based on hydrogen bonds, (iii) ionic interactions and (iv) π-π interactions (Fig. 1).

Various metal salts were applied within the aforementioned studies, it appeared that the following mordants improved the wash and light fastness values compared to the control sample: alum [13,14,19,22,25], alum in combination with ferrous sulfate [23], antimony potassium tartrate [21], ferrous chloride [18], ferrous sulfate [13,14,22,23], stannous chloride [14,17,20,24] and silver nanoparticles [15]. The main reason why metal salts are frequently used to improve the dye affinity is due to their ability to form metal-dye coordination complexes. Since anthocyanins and cellulose contain many hydroxyl groups with free electron pairs on the oxygen atoms, they could act as donors and fill the free orbitals of the metal ions. This induces a deprotonation upon forming the metal-ligand complex. Within literature, it has been stated that anthocyanins perform as bidentate ligands within metal complexation. The most important requirement for that, is the presence of hydroxyl groups at the $C_{3'}$ and $C_{4'}$ positions [11,27]. This leads to the conclusion that only three types of anthocyanins are able to form a coordination complex, i.e. cyanidin, delphinidin and petunidin. Furthermore, the formation of coordination complexes usually comes along with a bathochromic shift [27].

Meanwhile, research on the use of biomordants with anthocyanins increases gradually: tannic acid, a mixture of polygalloyl glucoses [16,20], and tannin [13] would increase the affinity of the substrate by means of van der Waals forces and hydrogen bonds [13]. These interactions originate from their large molecular size (500–3000 g mol^{-1}) and availability of hydroxyl groups, respectively. Next to that, the interaction between polysaccharides and anthocyanins has also emerged as one of the stabilizing mechanisms, e.g. gelation by alginate [28] or molecular inclusion [29]. The latter leads to cyclodextrins, which appear to possess promising properties for pigment inclusion via hydrogen bonding, van der Waals and electrostatic interactions [29,30].

The third mechanism involves developing anionic sites by cotton pretreatment. The generation of additional anionic sites is necessary as dyeing with an acidic dyebath includes a low pH. Hereby, the cellulosic hydroxyl groups are not sufficiently negatively charged to adsorb the flavylium cation. Therefore, dicarboxylic acids such as succinic acid [17] or a reactive anionic agent, based on 4-amino-benzenesulfonic acid and cyanuric chloride [16], are applied to establish ionic bonds with the flavylium cation.

The fourth mordanting method is based on copigmentation. This process is defined as the formation of noncovalent complexes by π-π interactions consisting of an anthocyanin and a copigment compound present within the source, and the accompanying changes in spectral properties such as absorption intensity and wavelength [11,31,32]. The major natural copigments are hydrolysable tannins, flavonoids and phenolic acids [31]. Within nature, anthocyanins exist as their acylated forms.

Due to intramolecular copigmentation, these acylated anthocyanins gain more stability in comparison to their unacylated forms. Diacylated anthocyanins result in a “sandwich” structure as the aromatic acyl moieties overlap with the benzopyrylium structure, which improves the

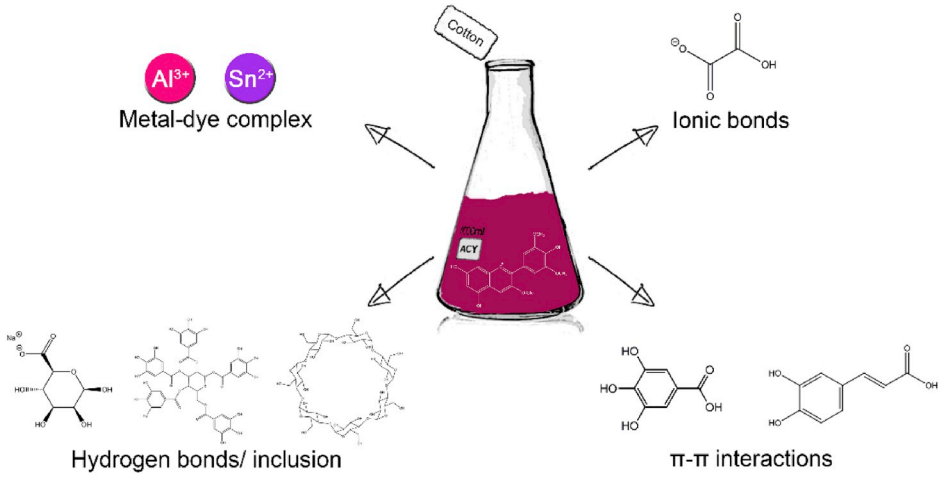

Fig. 1. The four typically proposed types of intermolecular interactions between anthocyanins and (bio)mordants. This paper therefore systematically compares: metal complexation: Sn(II) and Al(III), hydrogen bonds: sodium alginate, tannic acid and β-cyclodextrin; ionic bonding: oxalic acid; and π-π interactions: gallic acid and caffeic acid.

resistance to physicochemical and biochemical factors such as heat, light, pH changes, hydrogen peroxide and nucleophilic attack of water [32].

Apart from this diversity in mordanting techniques, little is known on the optimal conditions for dyeing with anthocyanins. In literature, different dyeing conditions were applied such as temperatures ranging from room temperature till 100 °C, different pH values between 2 and 5, dyeing time from 60 min till 24 h and different liquor ratios. Such a lack of consistency makes it difficult to compare literature, and furthermore it seems that there is a lack of evidence related to the optimized anthocyanin dyeing procedures.

For this purpose, this study contains an extensive experimental part on (i) the optimization of the dyeing procedure with anthocyanins for dyeing cotton and (ii) the investigation for effective (bio)mordants to improve the affinity of anthocyanins on cotton fibers by intermolecular interactions (e.g. metal-ligand, hydrogen bonds, ionic and π-π interactions), (iii) in combination with a modeling approach in the second part, presenting a profound understanding on the underlying mechanism between (bio)mordants, dye and substrate on molecular scale.

Through mathematical modeling, insight can be obtained in the sorption mechanisms and molecular modeling can greatly help in unravelling the underlying mechanisms governing the interactions between the dye and the (bio)mordant. Adsorption modeling with anthocyanins are frequently applied within purification methods. Hereby, different resins were compared for their adsorption and elution capacities [33]. Molecular modeling studies between metal-ions and anthocyanins involve a series of 12 common metallic cations in nature, where complexes of Co(III), Fe(III), Cr(III), and Al(III) were thermodynamically more favored [34,35]. Furthermore, the influence of the oxidation state of iron was investigated between malvidin-3-glucoside (mv-3-glc) and ellagic acid. Calculations show that Fe(II) preferably undergoes cation-π interactions, which are stronger than π-stacking [36]. Other studies based on anthocyanins were on conformational analyses [37–40], copigmentation effects of π-π interactions [31,41–43] and generation of UV-VIS spectra by time dependent-density functional theory (TD-DFT) [38,41]. Hereby, the behaviour of anthocyanins on intermolecular interactions and accompanying spectral changes due to copigmentation were clarified, but a systematic analysis of the four dyeing mechanisms is not available yet.

2. Materials and methods

2.1. Experimental section

2.1.1. Scope of the mordants

In this study, eight mordants were investigated to improve the affinity and stability of anthocyanins to cotton based on the four proposed types of intermolecular interactions as described above. Two metallic mordants were selected, supported by the successful application within literature, $SnCl_2$ and $AlK(SO_4)_2$. Other biomordants were selected according to the aforementioned intermolecular interactions they could undergo with anthocyanins. Tannic acid and sodium alginate for their hydrogen bonding. β-cyclodextrin is a funnel-shaped cyclic oligosaccharide with seven glucose moieties linked by α-(1–4) glycosidic bonds, and is particularly known for its inclusion capability of organic molecules. Oxalic acid was preferred for its low pKa values to form ionic bonds. Gallic acid and caffeic acid were selected to reproduce the stability obtained by copigmentation or π-π interactions.

2.1.2. Samples and reagents

Metallic mordants consist of tin chloride dihydrate (VEL) and potassium aluminium sulfate dodecahydrate (alum) (MERCK). The biomordants were oxalic acid dihydrate (Chem-lab), sodium alginate (PanReac Applichem), β-cyclodextrin (Acros organics), tannic acid (Sigma Aldrich), gallic acid (97.5–102.5% (titration), Sigma Aldrich) and caffeic acid (predominantly trans ≥ 99%, Acros organics). Hydrochloric acid (37% analytical reagent, Chem-lab) was used to acidify the extraction solvent. Sodiumhypophosphite (SHP) (Merck) was applied as a catalyst during the esterification reaction. A 50% sodium hydroxide solution (Sigma Aldrich) was used to adjust the pH of the dyebath. Potassium chloride (Chem-lab) and sodium acetate trihydrate (Chem-lab) were applied within the pH-differential method for determining the anthocyanin content. Spectrophotometric solutions are prepared in polystyrene macrocuvettes (VWR) with a path length of 1 cm. Cotton, with a density of 190 g m^{-2} and prepared for dyeing, was supplied by Utexbel NV and cut into samples, each weighing 1 g.

2.1.3. Extraction procedure

Blueberry waste would preferably be used if one is using the anthocyanins as natural colorant within the dyeing industry. However, for the experiments conducted, the use of blueberries as such or blueberry waste will not influence our results as the anthocyanins present are the same in both matrices. As for practical reasons, it was much easier to obtain blueberries as a rich source of anthocyanins than the blueberry waste. Therefore, the anthocyanins were extracted from the fruit itself. Frozen blueberries were crushed with pestle and mortar and extracted in acidic environment. The extraction made use of a material-to-liquor ratio (further referred to as M:L) of 1:3, i.e. 1 g of blueberry for 3 mL of solvent. The solvent consisted of a 1% (v/v) aqueous hydrochloric acid solution as dyeing occurs in aqueous environment. The extraction time and temperature were 1 h and 60 °C, respectively [44]. The solution was filtered through a Büchner funnel and filter paper with a 40 μm particle retention (VWR). The concentration of the filtrate obtained was 510.7 ± 9.5 mg malvidin-3-glucoside equivalents L^{-1} (hereinafter referred to as mv-3-glc equiv) and was used as dyebath (pH: 1.47). These conditions were made constant by dilution with the above-mentioned solvent to ensure consistent results. This simple cost-effective aqueous extraction was favored over methanol as dyeing commonly occurs within aqueous conditions and maximizing yield was not the main objective. Moreover, this avoids an additional evaporation or clean-up step to remove the organic solvent.

2.1.4. Optimization of dyeing conditions

The dyeing parameters, temperature, time, pH and concentration, were optimized for dyeing cotton without applying any mordant. The temperature was varied from 30 °C till 100 °C to find an optimum between dye uptake, color strength, degradation of the colorant and wash fastness. The duration time of dyeing was analyzed through adsorption kinetics whereby (0.5 mL) samples of the 100 mL dyebath were taken with a syringe for anthocyanin measurements at a 5-min interval from the beginning till 20 min, a 10-min interval till 60 min and a 30-min interval till 180 min. A blank dyebath was included to monitor the degradation at each stage. The pH optimization experiment consists of the dyebath being varied from the filtrate's pH till 11 by a 50% sodium hydroxide solution. The optimal concentration of the dyebath was also checked, and dilutions were carried out with a 1% HCl solution.

From preliminary tests, it was clear that only pre- and meta-mordanting dyeing procedures were taken into account as post-mordanting or after treatment of the dyed fabric resulted into leaching of the dye back into solution.

2.1.5. Premordanting procedure

The cotton samples were premordanted in a M:L of 1:50, i.e. 1 g of cotton fabric and 50 mL of distilled water. For both metallic mordants (coordination complexes), tin and alum and both polysaccharides (hydrogen bond interactions), sodium alginate and β-cyclodextrin, a concentration of 2 g L^{-1} was used, based on literature [17] and solubility restraints. The solutions used for the esterification reactions consisted of the (di)carboxylic acid and sodium hypophosphite (SHP, catalyst). For oxalic acid, gallic acid and caffeic acid, the concentrations were 50 g L^{-1}, 20 g L^{-1} and 2 g L^{-1}, respectively. An equal amount of SHP, 1:1 (w/w), was added and the pH of the solutions was adjusted to the

optimal pH for this reaction (pH = 3), which was only necessary for oxalic acid. The optimal premordanting condition for tannic acid was 25 g L^{-1} (50% o.w.f. and M:L of 1:20) at pH 7 [16], which was adjusted with a 50% sodium hydroxide solution. The temperature profile for premordanting was performed as described by Burkinshaw and Kumar (2010) [45]. The premordanted cotton samples were left air-dried overnight. These dried cotton samples were placed in 100 mL stainless steel beakers. The dye extract was added at a M:L ratio of 1:50 and placed within the Mathis Labomat BFA8 (40 rpm, auto reverse: 555). A temperature gradient of 2.0 °C min^{-1} was applied to obtain the optimal dyeing temperature of 80 °C, which continued to dye for 1 h. The samples were left air-dried for further analysis and testing. This premordanting procedure was performed in triplicate and each run was accompanied with a blank sample to monitor the potential compound specific degradation.

2.1.6. Metamordanting procedure

The mordant concentrations were similar compared to the premordanting procedure, but within metamordanting the distilled water has been replaced by the dye extract. The conditions for tannic acid remained similar except the pH of 7, which cannot be applied in this method as it would alter the dye's property. The biomordants requiring esterification were dyed at pH 3, which was the optimal pH for esterification. This metamordanting procedure was performed in triplicate and each individual mordant was accompanied with a blank sample to monitor the degradation.

2.1.7. Fourier-transform infrared spectrophotometer

The effectiveness of the mordants was investigated by infrared measurements (Figs. S2 and S3). Premordanted, dyed, wash- and light tested cotton samples were analyzed with the Nicolet iS50 ATR FT-IR spectrometer (Thermo Scientific). Each measurement consisted of 32 replicates and the wavenumber region ranged from 400 cm^{-1} till 4000 cm^{-1} with a wavenumber resolution setting of 4. The measured spectra were corrected for the baseline and normalized to the highest peak.

2.1.8. Spectrophotometric data

All spectrophotometric data (absorption and reflectance spectra) were measured with the PerkinElmer Lambda 900 UV/VIS/NIR Spectrometer. The dye uptake was monitored by measuring the anthocyanin concentration before and after dyeing by means of the pH-differential method [46]. Due to the high available content of mv-3-glc within blueberries [44,47,48] and the matching wavelength of maximum absorbance observed within the recorded UV-VIS absorption spectra, mv-3-glc was selected to express the anthocyanin concentration.

$$\text{Anthocyanin concentration}\left(\frac{\text{mg}}{\text{L}}\right) = \frac{\text{A}\cdot\text{MW}\cdot\text{DF}\cdot 1000}{\varepsilon\cdot\text{b}} \quad (1)$$

with absorbance $A = (A_{\lambda max} - A_{700\ nm})_{pH=1.0}$ - $(A_{\lambda max} - A_{700\ nm})_{pH=4.5}$, λ_{max} at 519 nm and the measurement at $\lambda = 700$ nm corrects for the haze within the solution. MW displays the molecular weight of mv-3-glc (493.44 g mol^{-1}), DF the dilution factor applied for the measurement, ϵ the molecular attenuation coefficient (28000 L mol^{-1} cm^{-1}) and b the path length of the cuvette (1 cm). This quantification method has been used to determine the (relative) exhaustion (E%) and the equilibrium adsorption capacity (q_e):

$$E\% = \frac{C_0 - C_e}{C_0}\cdot 100 \quad (2)$$

$$q_e = (C_0 - C_e)\frac{V_{solution}}{m_{fabric}} \quad (3)$$

in which, C_0 and C_e, define the initial and equilibrium dye concentrations (mg mv-3-glc equiv L^{-1}), respectively, q_e represents the amount of adsorbate per unit mass of adsorbent (mg mv-3-glc (g cotton)$^{-1}$), V, the volume of the dyebath (L) and m, the mass of the fabric (g). Due to the mediocre thermostability of anthocyanins, blank dyebaths were included along with the dyeing experiments. Hereby, the degradation factor can be assessed to correct the exhaustion and equilibrium adsorption capacity values (section S1.4). Next to that, structural properties of anthocyanins can be derived from the UV-VIS spectra such as the glycosylation level at the C_3 position, appearing as a shoulder in the 400–440 nm region [49,50]. This amount is defined by the ratio of absorbance values at 440 nm and λ_{max} ($A_{440\ nm}/A_{\lambda max}$), which accounts for 34.9 ± 0.6% within the dye extract. Furthermore, the half-life value $t_{1/2}$ was calculated by plotting the natural logarithm of the ratio of the anthocyanin concentration of the blank dyebath at specific times, as described within the optimization of the dyeing time, over the initial dye extract (C_t/C_0) as a function of time [51,52]. The slope of this plot yields the first-order rate constant k for which the half-life value can be determined with $t_{1/2} = (\ln 2)/k$.

Reflectance spectra were recorded, in triplicate, for dyed and wash- and light tested samples from 380 nm till 700 nm to obtain the color strength, which was calculated by the Kubelka–Munk equation:

$$\frac{K}{S} = \frac{(1-R)^2}{2R} \quad (4)$$

with K the absorption coefficient, S the scattering coefficient and R the reflectance. The K/S values were calculated by the integrated wavelength method.

Furthermore, these reflectance spectra were converted into the corresponding CIELAB coordinate system (L*, a*, b*, C* and h), with properties of a D65 illuminant and an observer angle of 10°, by OptLab-SPX software (Ascanis). L* represents the lightness of the sample, a* the red-green axis with a* > 0 red and a* < 0 green, b* the yellow-blue axis with b* > 0 yellow and b* < 0 blue, C* the chromaticity ($C^* = \sqrt{a^{*2} + b^{*2}}$) and h the hue angle ($h_{ab} = \arctan\left(\frac{b^*}{a^*}\right)$). The hue angle, which defines the color, around 0° (or 360°), 90°, 180° (or −180°) and 270° (or −90°) describes red, yellow, green and blue, respectively. The color difference, ΔE, is calculated between the tested sample and the dyed sample.

$$\Delta E^* = \sqrt{\left(L^*_{tested} - L^*_{dyed}\right)^2 + \left(a^*_{tested} - a^*_{dyed}\right)^2 + \left(b^*_{tested} - b^*_{dyed}\right)^2} \quad (5)$$

2.1.9. Fastness tests of dyed fabrics

Two standard methods of wash tests were applied on the cotton dyed samples: ISO105–C06 and ISO105-E01. The former is based on the use of detergent (ECE formulation phosphate reference detergent (B) without optical brightening agent, pH = 9.4), while the latter is only based on water. The assessment whether the natural dye had completely been washed away after the ISO105–C06 test or was still present within the fabric, includes the reimmersion of the washed cotton sample in a 1% HCl solution at a similar liquor ratio as dyeing, for 1 min. In order to assess staining, James Heal multifibers were stitched to the dyed cotton samples prior to testing. The ISO105–C06 tests were carried out in a James Heal Gyrowash 815/8. Afterwards, the washed samples were left air-dried. The color fastness to light was tested with ISO105–B02, using a Xenotest Alpha instrument. The samples were irradiated for 22 h and had an radiant exposure H of 3350 kJ m^{-2}. All fastness values of the tested fabrics were examined by a James Heal grey scale for assessing staining ISO105-A03 and grey scale change in color ISO105-A02 (1–5) in a light box with D65 illumination. The fastness values of the light test for color change were evaluated by blue wool standards (1–8).

2.1.10. Statistical analysis

The one-way analysis of variance (ANOVA) was carried out to investigate the influence of the (bio)mordants with respect to the control sample by comparison of means. The significance level for the statistical

analyses is 0.05. The p-values obtained lower than 0.05 are regarded as significantly different. All statistical analyses were performed with SPSS Statistics Version 25 (IBM) software.

2.1.11. Adsorption models

Adsorption isotherms describe the mobility and affinity of an adsorbate within an aqueous environment to a solid-phase at constant temperature and pH [53]. The experimental adsorption equilibrium data were collected as mg mv-3-glc equiv per gram of cotton, which is the most abundant compound within blueberries, under optimized dyeing conditions and without mordant. These single component data were fitted with two two-parameter models, Langmuir and Freundlich, and two three-parameter models, Redlich-Peterson and Sips. Describing multicomponent adsorption is frequently performed by means of ideal adsorbed solute theory (IAST). This multicomponent adsorption model generates good predictions for mixtures that are close to ideal and mixtures containing compounds with similar adsorption affinities. However, the main shortcomings of this model are predicting adsorption equilibria of mixtures containing molecules of different size, polarity or adsorption interactions (affinities) such as the blueberry extract, and the poor predictions due to adsorbent heterogeneity [54]. Table 1 contains the mathematical expressions of the models applied, q_e and C_e represent the amount of adsorbate per unit mass of adsorbent (mg mv-3-glc equiv (g cotton)$^{-1}$) and the equilibrium dye concentration (mg mv-3-glc equiv L^{-1}), respectively. The isotherm parameters for Langmuir are K_L, the isotherm constant (L (mg mv-3-glc equiv)$^{-1}$), and Q_L, the maximum monolayer adsorption capacity (mg mv-3-glc equiv (g cotton)$^{-1}$); for Freundlich: K_F the adsorption capacity (mg mv-3-glc equiv$^{1-1/n}$ $L^{1/n}$ (g cotton)$^{-1}$) and n_F, the adsorption intensity; for Redlich-Peterson: K_R Redlich-Peterson isotherm constant as L (g cotton)$^{-1}$, a_R, Redlich-Peterson isotherm constant as (L (mg mv-3-glc equiv)$^{-1}$)$^{\beta}$ and β, the exponential variable; and for Sips model: K_s (L (g cotton)$^{-1}$), a_S (L (mg mv-3-glc equiv)$^{-1}$) and n_S the Sips model exponent.

Table 1
An overview of the isotherm and kinetic models applied.

Adsorption model	Definition	Plot	Assumed mechanisms	Ref.
Isotherm				
Langmuir	$q_e = \frac{Q_L K_L C_e}{1 + K_L C_e}$	$\frac{1}{q_e}$ *vs* $\frac{1}{C_e}$	Monolayer adsorption, identical sites and no mutual interactions between neighbouring adsorbed molecules	[53,55]
Freundlich	$q_e = K_F C_e^{1/n_F}$	$\ln q_e$ *vs* $\ln C_e$	Multilayer adsorption of the molecules on a heterogeneous surface	[53,56]
Redlich-Peterson	$q_e = \frac{K_R C_e}{1 + a_R C_e^{\beta}}$	q_e *vs* C_e [(a)]	Describe wide concentration range for homogenous and heterogeneous systems	[53,57]
Sips	$q_e = \frac{K_S C_e^{n_s}}{1 + a_S C_e^{n_s}}$	q_e *vs* C_e [(a)]	Low adsorbate concentrations: Freundlich, while high concentrations: Langmuir	[53,58]
[(a)] Iterative fitting was performed for this model				
Kinetics				
Lagergren	$\frac{dq_t}{dt} = k_1(q_e - q_t)$	$\ln(q_e - q_t)$ vs t	Adsorption reaction model	[59–61]
Pseudo-second order	$\frac{dq_t}{dt} = k_2(q_e - q_t)^2$	$\frac{t}{q_t}$ *vs* t	Adsorption diffusion model	[59–63]
Intraparticle diffusion model (IPD)	$q_t = k_P t^{\frac{1}{2}} + C$	q_t *vs* $t^{\frac{1}{2}}$	Three-step process: 1) external surface adsorption, 2) gradual adsorption step where intraparticle diffusion is controlled and 3) equilibrium stage	[59,60,64]

These nonlinear isotherm models were solved by iteration in Origin (OriginLab, Northampton, MA). In order to determine the best isotherm model to describe the uptake of anthocyanins on cotton, the Chi-square analysis was carried out as goodness of fit next to R^2-values. The Chi-square test is calculated as the sum of squares of the differences between the experimental data and the data fitted by the model:

$$X^2 = \sum \frac{(q_{e,exp} - q_{e,m})^2}{q_{e,m}} \quad (6)$$

with $q_{e,exp}$ (mg mv-3-glc (g cotton)$^{-1}$) and $q_{e,m}$ (mg mv-3-glc (g cotton)$^{-1}$) the equilibrium adsorption capacities from the experimental data and the isotherm model, respectively [65]. A small X^2 value is obtained when the data of the model is similar to the experimental data, when they differ X^2 will be large.

2.2. Molecular modeling details

2.2.1. Static calculations

In order to study the metal-dye coordination complexes and ionic interactions between oxalic acid and mv-3-glc, static calculations were carried out with Gaussian16 [66] by means of density functional theory (DFT). Geometrical optimizations were performed with the B3LYP functional, with a 6–311++G(d,p) basis set [67,68], as it has proven its reliability for a broad set of chemical systems [34,69]. Furthermore, Grimme's third-generation dispersion corrections were also added to account for the dispersion interactions [70]. As dyeing occurs in an aqueous environment, implicit solvation was taken into account by the standard self-consistent reaction field using the integral equation formalism variant of the polarisable continuum model (IEF-PCM) with water as solvent ($\varepsilon = 78.3553$) [71].

Static calculations were performed to investigate the interaction of the dye with a series of metal coordination complexes. Both complexes with aluminium and tin were considered, which were modelled using an effective core potential DEF2TZVPP basis set.

The following systems were considered:

$$Sn(IV)Cl_2 + 2\ \ Dye^- \rightarrow\ \ Sn(IV)(Dye)_2Cl_2 \quad (7)$$

$$Al(H_2O)_6^{3+} + 1\ \ Dye^- \rightarrow\ \ [Al(Dye)(H_2O)_4]^{2+} + 2\ \ H_2O \quad (8)$$

$$Al(H_2O)_6^{3+} + 2\ \ Dye^- \rightarrow\ \ [Al(Dye)_2(H_2O)_2]^{+} + 4\ \ H_2O \quad (9)$$

$$Al(H_2O)_6^{3+} + 3\ \ Dye^- \rightarrow\ \ Al(Dye)_3 + 6\ \ H_2O \quad (10)$$

In the literature, it has been shown that stannic chloride (Sn(IV)) will be formed by oxidation at the expense of stannous chloride (Sn(II)) and hydrochloric acid [72]. The structural organotin(IV) complexes are potentially tetrahedral, trigonal pyramidal, or octahedral, following the R_nSnX_{4-n} formula (n = 1–3, X = halide, carboxylate, dithiocarbamate etc.) [73,74]. The typical coordination geometry observed between diorganotin(IV)$^{2+}$ and flavonoids containing vicinal hydroxyl groups is the octahedral configuration (O_h4) [75]. Therefore, the octahedral $SnCl_2$ complex consists of the metal salt attached to two bidentate dye ligands (Equation (7)). The aluminium ion is represented as a metal aquo complex, i.e. an Al(III) cation surrounded by six water molecules in an octahedral fashion. To investigate the stability of the aluminium-anthocyanin complex, two water molecules from the initial metal aquo complex have been exchanged by one bidentate anthocyanin (Equations (8)–(10)) till all water molecules were substituted by the natural dyes [34]. The anthocyanins eligible for complexation are cyanidin-3-glucoside, delphinidin-3-glucoside and

petunidin-3-glucoside (hereinafter referred to as cy-3-glc, dp-3-glc and pt-3-glc, respectively), due to the presence of vicinal hydroxyl groups at the B-ring. The global charge of the ligands used within these coordination complexes is −1. This is obtained after deprotonation of two hydroxyl groups at the 3′ and 4' positions of the flavylium cation.

Intermolecular interactions between oxalic acid and mv-3-glc were investigated under the same conditions as the geometrical optimizations. The resulting interaction energies from these static calculations were corrected for Basis Set Superposition Error (BSSE). For these static PCM calculations, counterpoise correction was applied to the PCM optimized structures in separate calculations without implicit solvation, as the aforementioned correction cannot be implemented during PCM calculations [76]. Furthermore, charge distribution and atomic population analyses of the flavylium cation, mv-3-glc and oxalic acid were carried out with Hirshfeld I (HI) [77] and Minimal Basis Iterative Stockholder (MBIS), an expanded variant of the Hirshfeld AIM method [78]. HI is able to create a good estimate of the electrostatic potential of organic molecules [79]. Both were performed using the in-house software package HORTON 2.1.1 [80].

2.2.2. Molecular dynamic simulations

In addition to static calculations based on DFT, semi-empirical molecular dynamic (MD) simulations were carried out to investigate the intermolecular behaviour between tannic acid and mv-3-glc by using the CP2K software [81] as tannic acid is a considerably large system, it was not feasible to treat this system at the DFT level. The unit cell, measuring 40 Å × 40 Å x 40 Å, contained tannic acid and mv-3-glc and was simulated by PM6 with Grimme D3 dispersion corrections [82]. For these simulations, the canonical ensemble was applied at 353 K controlled by a CSVR thermostat with a time constant of 300 fs. A time-step of 0.5 fs is used for the integration of the equation of motion. The self-consistent field (SCF) convergence criterion was fixed at 10^{-5} eV. The total run time for this simulation was 305 ps, the initial 50 ps were omitted by cause of equilibration.

In a second stage, as solvent effects could highly influence the interaction patterns between mordant and dye, solvation has been taken into account in an explicit manner in order to match the experimental conditions more realistically. To this end, classical molecular dynamics simulations are performed on a GPU cluster. Therefore, both tannic acid and the mv-3-glc dye were solvated with water molecules to reproduce the experimental density and accounting two solvent layers of water for each molecule (based on the experimental radial distribution function of water) [83]. This resulted in a solute-water box of 53 Å × 53 Å x 53 Å counting 4892 water molecules per solvation layer, generated with PACKMOL [84]. Both compounds were parameterized with the GAFF2 force field using AmberTools [85,86] and the TIP3P water model [87], which has proven its accountability in several researches [88]. The simulation was performed in the NpT ensemble, which was controlled by the Langevin integrator and Monte Carlo barostat (1 bar) [89]. The total duration of the simulation was 2294.5 ns and analysis of the trajectory files was accomplished, by using the last 1657.6 ns of the MD simulation, with the MDTraj python package [90] and PLUMED software package [91].

3. Results and discussion

This section will first discuss the optimization of the dyeing procedure for anthocyanins on cotton without applying any mordant. Next, the experimental data on the influence of the (bio)mordants are described, which are elaborated according to the interaction mechanism. Finally, observations from the dyeing experiments are clarified with the results obtained from modeling.

3.1. Optimization of the dyeing parameters

3.1.1. Temperature

Firstly, the influence of the temperature has been studied. Hereby, the dye uptake has been monitored over a temperature range from 30 °C till 100 °C. As anthocyanins are susceptible to degradation at higher temperatures [92], a compromise should be found between dye uptake, color strength, degradation of the colorant and wash fastness (Table S1). From Fig. 2A, it can be seen that dyeing at 80 °C resulted into the highest dye uptake. Table S1 shows that dyeing at temperatures lower than 60 °C resulted in a high color strength and a negligible amount of degradation, but had a larger color loss after washing. The dyeing properties at 70 °C and 80 °C were very similar, with the dye uptake as the most determining factor for the latter even though a small amount of degradation is present. In general, the thermal stability of anthocyanins is determined by the grade of methoxylation, glycosylation and acylation [93,94]. This is advantageous for the high content of mv-3-glc present within blueberries, while other anthocyanin derivatives are more prone to thermal degradation. This implies that dyeing at 80 °C just reached the equilibrium between maximum dye uptake and the initial steps of anthocyanin degradation, which are the successive deglycosylation reactions. This results into their respective aglycones, which still possess color and eventually lead to cleavage into a phenolic acid and a phenolic aldehyde [95]. These two latter stages are more pronounced at 90 and 100 °C dyeing. Dyeing at 90 °C still resulted in a high dye uptake, however, a color loss on the fabric was observed due to the degradation of anthocyanins, that was already taken up within the fabric, leading to a lower a* and higher L* value compared to lower dyeing temperatures. This decline in color loss was larger for the sample dyed at 100 °C. Therefore, 80 °C has been applied in further experiments.

3.1.2. Dyeing time

The dyeing time was monitored by performing an adsorption kinetics experiment whereby the dye uptake has been investigated in function of time. Hereby, Fig. 2B illustrates that the dye uptake reached a plateau after 60 min of dyeing at 80 °C, indicating that dyeing attains equilibrium and longer dyeing times are not required.

As mentioned above, the blueberry extract consists of glycosides and aglycones. The former shows higher solubility within water, while the latter is more soluble in alcohol [96]. Through this experiment, the amount of 3-glycosides within the blueberry extract was determined by the $A_{440\ nm}/A_{\lambda max}$ as a function of time. Fig. 2C illustrates the increase of this ratio over time. As the optimal dyeing time is 60 min, the ratio is barely 3% higher compared to the initial dyebath, while it reaches up to 14% at the end of this experiment. Two processes can occur within the blank dyebath: the 3-glycosides are degraded by losing their sugar moiety and become aglycones and the degradation of aglycones into their corresponding phenolic constituents. Both aforementioned processes also occur within the sample beaker, with the additional factor of the uptake of anthocyanins and anthocyanidins into the fabric. The increase of 3% after dyeing is too low to draw any conclusion. However, the 14% increase of the ratio at the end of the kinetic experiment can be ascribed to the higher rate of degradation of aglycones compared to 3-glycosides, meaning the latter being more stable despite the acidic conditions and elevated temperature. This is also indicated in Fig. 2D, which displays the change of absorbance at the wavelength of maximal absorption (519 nm) and the wavelength determining the fraction of 3-glycosides (440 nm) as a function of time. Even though a decline is noticed for both peaks, the absorbance value at 440 nm decreases more slowly compared to the total anthocyanin peak, while the ratio between them increases. Furthermore, the half-life value of the dyebath, 1.88 h, determined by first-order reaction kinetics (Fig. S5), showed the same order of magnitude as the half-life values obtained by Yue and Xu (2008) [52] with bilberry extract heating at 80 °C and Sadilova et al. (2007) [51] for strawberry and elderberry at pH 3.5 and a temperature of 95 °C.

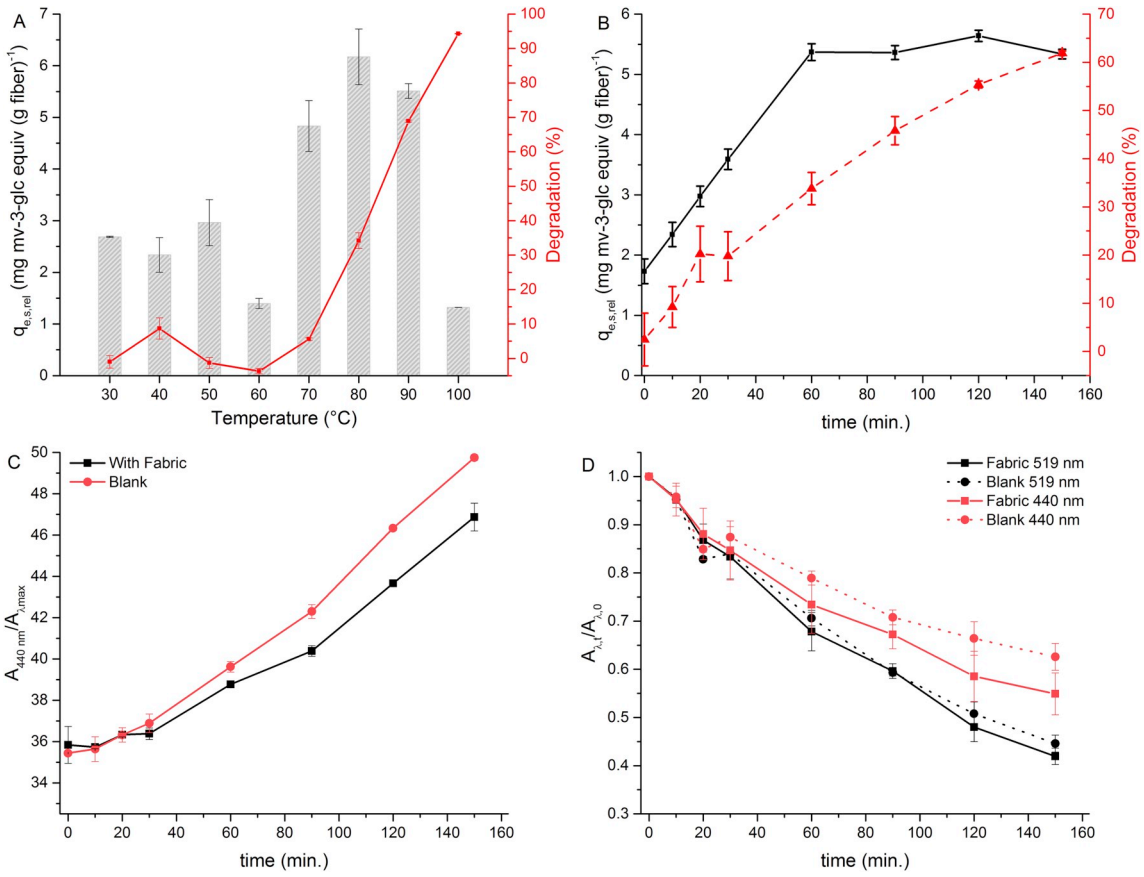

Fig. 2. A: the optimization of the dyeing temperature in terms of relative dye uptake and amount of degradation, B: the relative dye uptake measured at 80 °C and the extent of degradation as a function of time, C: the $A_{440\ nm}/A_{\lambda,max}$ ratio representing the 3-glycosylation level of the dyebath over time and D: the absorbance ratio over time for two wavelengths (440 nm and 519 nm) of a blank dyebath and one containing the fabric.

Table 2
Colorimetric values and color strength of fabrics dyed at different pH conditions and concentrations of the dye extract (uncertainties expressed as standard deviation (n = 3)).

	After dyeing							After washing ISO105 C06						
pH	L*	a*	b*	C*	h	K/S	Samples	L*	a*	b*	C*	h	K/S	ΔE	Samples
1.47	47.9 ± 0.9	26.4 ± 0.6	-5.3 ± 0.2	26.9 ± 0.6	348.7 ± 0.7	1.8 ± 0.1		72.1 ± 0.2	2.0 ± 0.2	1.7 ± 0.6	2.6 ± 0.5	44.3 ± 8.8	0.3 ± 0.1	35.1 ± 1.1	
3	49.9 ± 0.6	22.4 ± 0.8	-6.7 ± 0.2	23.3 ± 0.9	343.4 ± 0.1	1.5 ± 0.1		73.8 ± 0.7	1.7 ± 0.1	1.6 ± 1.0	2.4 ± 0.7	51.5 ± 1.1	0.3 ± 0.1	32.7 ± 1.3	
5	62.6 ± 0.1	3.5 ± 0.1	-2.5 ± 0.2	4.3 ± 0.2	324.6 ± 1.2	0.7 ± 0.1		74.8 ± 0.2	1.3 ± 0.1	0.7 ± 0.1	1.5 ± 0.1	29.4 ± 1.9	0.3 ± 0.1	12.7 ± 0.2	
7	72.9 ± 1.3	3.7 ± 0.6	18.1 ± 1	18.4 ± 1.1	78.6 ± 1.2	0.5 ± 0.1		82.4 ± 0.7	3.3 ± 0.4	8.3 ± 0.6	9.0 ± 0.7	68.6 ± 1.0	0.1 ± 0.1	13.6 ± 0.7	
9	72.5 ± 0.3	2.0 ± 0.4	14.6 ± 1.1	14.7 ± 1.2	82.4 ± 1.0	0.5 ± 0.1		84.1 ± 0.6	2.5 ± 0.2	6.9 ± 0.5	7.3 ± 0.5	70.3 ± 0.3	0.1 ± 0.1	14.0 ± 1.0	
11	79.5 ± 0.6	3.5 ± 0.2	14.5 ± 0.9	14.9 ± 0.9	76.3 ± 0.2	0.2 ± 0.1		89.3 ± 0.1	1.2 ± 0.1	5.9 ± 0.1	6.0 ± 0.1	78.5 ± 0.0	0.1 ± 0.1	13.2 ± 1.0	
Dilution															
Original[a]	47.4 ± 0.9	26.6 ± 0.6	-5.6 ± 0.4	27.2 ± 0.5	348.2 ± 0.9	1.9 ± 0.1		69.3 ± 0.3	-1.8 ± 0.4	0.1 ± 0.6	1.9 ± 0.4	179.9 ± 19.4	0.5 ± 0.1	36.3 ± 0.8	
2-fold[a]	53.5 ± 0.3	24.8 ± 0.2	-7.0 ± 0.1	25.8 ± 0.2	344.2 ± 0.3	1.2 ± 0.1		73.2 ± 0.1	-2.1 ± 0.2	-0.1 ± 0.5	2.2 ± 0.2	184.1 ± 12.1	0.3 ± 0.1	34.1 ± 0.4	
5-fold[a]	63.1 ± 0.3	21.2 ± 0.3	-7.5 ± 0.1	22.5 ± 0.3	340.4 ± 0.3	0.6 ± 0.1		78.9 ± 0.2	-2 ± 0.3	0.2 ± 0.2	2 ± 0.3	174.7 ± 4.6	0.2 ± 0.1	29.1 ± 0.2	
10-fold[a]	68.5 ± 0.1	19.1 ± 0.3	-7.3 ± 0.1	20.4 ± 0.3	339 ± 0.1	0.4 ± 0.1		82.2 ± 0.5	-2.1 ± 0.2	0.7 ± 0.3	2.2 ± 0.3	161.0 ± 5.6	0.1 ± 0.1	26.4 ± 0.5	

[a]: the concentrations for the original, 2-, 5- and 10-fold diluted extract were: 510.7 ± 9.5, 257.1 ± 7.7, 69.3 ± 1.1 and 40 ± 0.4 mg mv-3-glc L^{-1}, respectively.

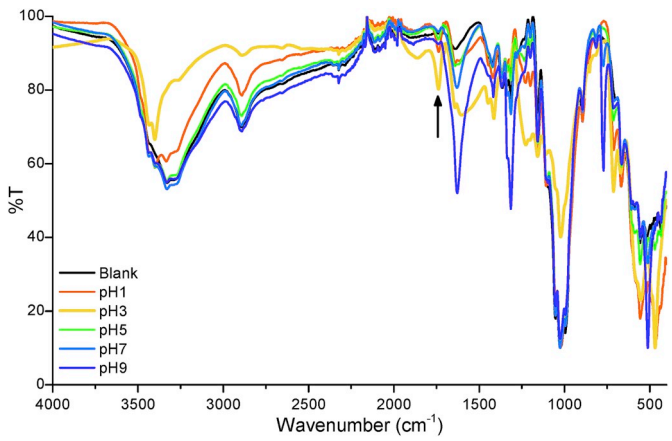

Fig. 3. Infrared spectra of esterification reactions with oxalic acid at different pH conditions.

3.1.3. pH

The stability of anthocyanins for dyeing was also studied. Due to the fact that anthocyanins are pH-sensitive, the pH of the dyebath was altered from 1.47 till 11 and dyed at 80 °C for 60 min. Hereby, Table 2 shows that the color strength is highest for the pH of the original extract (pH = 1.47), followed by dyeing at pH 3. At increasing pH, the dyebath consisted of a mixture of different anthocyanin isomers and not exclusively the flavylium cation. At pH 5, the a* value decreased significantly and the fabric displays a bluish tint. Dyeing at pH 7 and beyond, the degradation of these isomers occurs more rapidly at higher temperatures. This resulted into yellow degradation products of anthocyanins, hence the positive b* color value. This was evidenced by the fact that no color change was visible when the fabrics were placed in a 1% HCl solution, indicating the presence of degradation products (i.e. phenolic acid and phenolic aldehyde) rather than the chalcone isomer [51,95]. Therefore, the pH of the original extract remains unadjusted for further dyeing experiments.

3.1.4. Concentration

The concentration of the dyebath was also optimized in terms of color strength. Dilutions of the original extract were made with a 1% HCl solution. It was observed that a higher dilution factor results in a decline of redness (a*), an increase in L* and lower K/S values (Table 2). The smaller color differences (ΔE) are due to the fact that the initial dyed cotton samples already possess high lightness values. This experiment showed that lower concentrations of the dyebath were not sufficient to saturate the cotton fabrics with the dye, hence the lower color strength.

3.1.5. Esterification

In order to create anionic sites on the cotton fabrics, an optimal esterification reaction was developed with oxalic acid. Literature shows that SHP is the most efficient catalyst for this reaction [97,98]. To effectively verify the formation of the ester peak, the premordanted fabrics were rinsed with grade 3 water in the same M:L ratio. The FT-IR spectra showed that rinsing reduced the amount of ester bonds formed, but they still remain within the cotton (section S1.7). The anionic sites formed can potentially attract the dye molecule through ionic bonds and strengthen its affinity. The effect of the pH for this reaction was investigated as oxalic acid has two pKa values, 1.25 and 4.14. The most interesting peaks of cellulose to investigate are at 3326 cm^{-1} (O–H stretch), 2888 cm^{-1} (symmetric C–H stretch), 1632 cm^{-1} (OH bend of absorbed water), 1423 cm^{-1} (in-plane HCH and OCH bending vibration), 1368 cm^{-1} (in-plane CH bending), 1313 cm^{-1} (CH_2 rocking vibration at C_6), 1157 cm^{-1} (C–O–C asymmetrical stretch) and 1020 cm^{-1} (C–C, C–OH, C–H ring and side group vibrations) (Fig. 3) [99]. At pH 1, the peak at 1735 cm^{-1} (C═O stretch) and an increased peak 1157 cm^{-1} (C–C–O stretch of an ester bond) indicate that oxalic acid, as a dicarboxylic acid, was able to form an ester bond. At pH 3, oxalic acid exists as hydrogen oxalate and several variations in peak intensities illustrate the increased formation of ester bonds with the availability of anionic sites: an increase at 1735 cm^{-1} (ester bond), a decrease of vacant hydroxyl groups shown by 3326 cm^{-1} and 1020 cm^{-1} (primary alcohol), and an increase at 1414 cm^{-1} and 1600 cm^{-1} (symmetric and asymmetric CO_2 stretch, respectively). Beyond pH 5, oxalic acid exists entirely as dicarboxylate, which could be seen around 1600 cm^{-1} (asymmetric CO_2 stretch) and 1313 cm^{-1} (C–O stretch). Both peaks intensify with increasing pH. The C═O stretch is small at pH 5 and absent at pH 7 and 9. From this FT-IR analysis, it can be concluded that pH 3 offers the most effective esterification. This is in good agreement to the optimal pH found by Yang (1993) [97] for ester crosslinking of cellulose with a polycarboxylic acid.

3.2. Dyeing results with (bio)mordants, color measurement and fastness

3.2.1. Metallic mordants (tin and aluminium)

The first approach to improve the affinity of anthocyanins for cellulose, which could be seen as a non-preferable reference, is the application of metallic mordants. The mordants of interest were stannous chloride and alum. Under optimized dyeing conditions, the relative dye uptake, $q_{e,s,rel}$, for the premordanted tin sample is 27% more compared to the control sample (Table 3). This higher dye uptake can also be translated towards the colorimetric coordinates whereby the premordanted stannous chloride cotton sample showed a significant darker purple color, lower L*, a* and more negative b* values, compared to the control sample ($F(1,4) = 75.81$, $p = 0.0010$; $F(1,4) = 11.80$, $p = 0.026$ and $F(1,4) = 7.97$, $p = 0.048$; respectively). Furthermore, the largest color strength is also notable for the premordanted tin sample, 5.2 compared to 2.1 for the control sample ($F(1,4) = 34.52$, $p = 0.004$). Within metamordanting, tin resulted in a lighter purple shade compared to the premordanted sample. This was also visible at the maximum absorption peak that was bathochromatically shifted to 528 nm compared to the blank (Fig. S7). The aluminium mordant did not show any color difference in pre- or metamordanting dyeing compared to the blank in every aspect ($p > 0.05$). During the wash tests, most of the samples turned bluish/grey due to the alkaline detergent of the ISO105–C06 test, explained by the dye's pH sensitivity, but the premordanted tin sample still maintains an intense purple tint (L*: 48.9, a*: 2.2 and b: -5.9). The color difference, ΔE_1, is also lower compared to the control, assuming the main effect is related to the pH of the detergent rather than washing off. An indicator of the presence of the dye within the fabric, is by performing the reimmersion test (Table 4). It can be seen that both tin mordanted samples still holds a significant amount of anthocyanins (pre: L* 50.6, a* 17.3 and b* −13.2 ($F(1,4) = 122601$, $p < 0.001$; $F(1,4) = 21952$, $p < 0.001$; $F(1,4) = 18336$, $p < 0.01$; respectively); meta: L* 71.7, a* 8.5 and b* −4.7 ($F(1,4) = 268$, $p < 0.001$; $F(1,4) = 5547$, $p <$

Table 3
The relative exhaustion levels ($E_{s,rel}$) and relative equilibrium adsorption capacities ($q_{e,s,rel}$) of the dyebaths (uncertainties expressed as standard deviation (n = 3)).

	Premordanting		Metamordanting	
	$E_{s,rel}$ (%)	$q_{e,s,rel}$ (mg dye/g fiber)	$E_{s,rel}$ (%)	$q_{e,s,rel}$ (mg dye/g fiber)
Control	25.1 ± 1.2	6.1 ± 0.2	25.1 ± 1.2	6.1 ± 0.2
$SnCl_2$	33.4 ± 0.7	7.8 ± 0.3	20.9 ± 0.9	5.5 ± 1.0
Alum	25.6 ± 0.1	5.9 ± 0.9	23.5 ± 1.2	6.2 ± 1.3
Tannic acid	23.5 ± 1.7	5.5 ± 0.6	26.7 ± 0.7	7.0 ± 1.2
β-CD	24.5 ± 0.8	6.0 ± 0.7	22.9 ± 1.1	5.9 ± 0.7
Alginate	24.2 ± 1.2	5.9 ± 0.6	22.7 ± 1.2	5.9 ± 1.1
Oxalic acid	22.1 ± 0.2	4.5 ± 0.8	31.0 ± 0.1	6.9 ± 0.1
Gallic acid	22.6 ± 1.0	5.2 ± 0.3	14.1 ± 0.5	4.1 ± 0.2
Caffeic acid	24.9 ± 1.3	5.8 ± 0.7	33.2 ± 1.4	8.4 ± 1.3

0.001; F(1,4) = 8192, p < 0.001; respectively)). This also resulted into a higher color strength and a higher color difference, ΔE_2 (relative to washed samples), which is mainly contributed by the a* value. The reimmersed alum samples did not show any significant differences compared to the reimmersed control sample as the dyed samples did not show any added value after dyeing in the first place. In Table 5, the color fastness to water is displayed. In general, it can be seen that the colors are better retained on the fabrics, now the detergent has been omitted, but it still marks the hydrophilicity of the dye. Both tin mordanted samples retain their color more strongly compared to the control sample (pre: L* 30.7, a* 14.3 and b* −13.1 (F(1,4) = 1780, p < 0.001; F(1,4) = 0.10, p = 0.766; F(1,4) = 697, p < 0.001; respectively); meta: L* 46.4, a* 15.0 and b* −13.5 (F(1,4) = 30, p = 0.005; F(1,4) = 0.67, p = 0.46; F(1,4) = 1853, p < 0.001; respectively)), although the lightness (L*) of the metamordanted sample is slightly higher. The water test on alum mordanted samples show comparable properties to the control sample. The general trend in fastness values are low staining on the multifiber and a high color change for ISO105–C06 and the opposite for ISO105-E01, larger staining on the multifiber and smaller color change were observed. The metamordanted alum shows a better fastness than its premordanted analogue. The best result for color change is the premordanted tin sample in both wash tests (Table 6). Next to that, the light test results also show that the premordanted tin sample is capable to retain its color better than the aluminium and control sample, based on the ΔE and fastness value. This is in good agreement with the observations made by Wang et al. (2016) [17], where $SnCl_2$ retained its color better and slightly better after one washing cycle in neutral and alkaline soapy solution, respectively, in comparison to the control sample. The use of alum in other studies resulted in a more greyish and lightly blue tinted samples, however different pH and fibers were used [13,14,22]. Next to that, the fastness values with alum were comparable with the control samples. From this section, it can be concluded that tin improves the stability and affinity of anthocyanins for cotton, although it is not likely to be first choice for application purposes due to its potential health and environmental hazards.

3.2.2. Biomordant: hydrogen bonds

Three biomordants, tannic acid, sodium alginate and β-cyclodextrin, were investigated for their potential intermolecular interactions through hydrogen bonding as these compounds contain vast amounts of hydroxyl groups. The dye uptake of these compounds did not indicate any significant improvement compared to the control sample (Table 3). Premordanted tannic acid cotton sample showed a yellowish color after the pretreatment, which indicates the successful application on it. The FT-IR spectra verified the presence of tannic acid with increments visible at the at 3325 cm^{-1} (OH-stretch), 2888 cm^{-1} (symmetric C–H stretch), 1700 cm^{-1} (conjugated aromatic ester C═O stretch), 1610 cm^{-1} (aromatic C═C stretch), 1313 cm^{-1} (CH_2 rocking vibration at C_6) and 1200 cm^{-1} (C–C–O conjugated aromatic ester stretch) (Figs. S2B and S3B). The dyed premordanted tannic acid sample produces a better color strength (K/S = 2.7). Meanwhile, the metamordanted tannic acid sample produces a very bright color, which is indicated by a combination of slightly higher L* value and a more positive a* value (a*: 38.3). The λ_{max}-value shifted towards a higher wavelength (524 nm) as a consequence of the copigmentation effect (Fig. S7). After the detergent wash step, the pre- and metamordanted tannic acid sample still shows a feeble yellow tint, which still holds during the reimmersion step (positive b* value) (Table 4). For the fastness to water, the metamordanted sample still displays a more intense red color as it was initially more brighter than the other mordants. However, this decay (ΔE) is situated in the same range compared to the other mordants. The increased redness (a* value) and K/S value of the premordanted 30% and 50% o.w.f tannic acid dyed cotton samples were also observed within Bechtold et al. (2007) [13] and Wang et al. (2016) [17]. In terms of fastness levels, tannic acid matches the control sample and marks a half grade better for color change after the water-based wash test. Additionally, tannic acid showed very good fastness values for the light test in both dyeing procedures ΔE = ± 15.0 (Table 5), which confirms the observations found

Table 4
The colorimetric properties (D65/10) and color strength of dyed (pre- and metamordanted), washed (according to ISO105–C06 and reimmersed cotton samples (uncertainties expressed as standard deviation (n = 3)). Color differences ΔE_1 and ΔE_2 are calculated with respect to dyed and washed fabrics, respectively.

	After Dyeing							After Washing ISO105-C06								After washing ISO105-C06 and reimmersion in a 1% HCl solution							
Premord.	L*	a*	b*	C*	h	K/S	Samples	L*	a*	b*	C*	h	K/S	ΔE_1	Samples	L*	a*	b*	C*	h	K/S	ΔE_2	Samples
Control	46.2 ± 1.3	29.1 ± 3.0	-4.7 ± 0.8	29.5 ± 2.8	350.7 ± 2.5	2.1 ± 0.2		70.7 ± 1.4	0.2 ± 1.9	0.7 ± 0.8	1.7 ± 1.0	42.1 ± 4.1	0.4 ± 0.1	36.2 ± 1.1		75.6 ± 0.4	4.2 ± 0.1	-0.5 ± 0.1	4.2 ± 0.1	353.7 ± 0.8	0.4 ± 0.1	6.5 ± 2.3	
$SnCl_2$	31.1 ± 2.7	20.5 ± 3.1	-6.5 ± 0.7	21.6 ± 3	342.3 ± 2.5	5.2 ± 1.2		48.9 ± 2.5	2.2 ± 1.8	-5.9 ± 0.9	6.3 ± 1.5	289.1 ± 13.1	1.6 ± 0.3	26.2 ± 0.5		50.6 ± 0.2	17.3 ± 0.1	-13.2 ± 0.2	21.8 ± 0.2	322.5 ± 0.2	1.3 ± 0.1	15.3 ± 0.3	
Alum	46.8 ± 1.6	28.4 ± 1.7	-5.3 ± 0.9	28.9 ± 1.5	349.4 ± 2.4	2.0 ± 0.2		72.2 ± 2.7	-1.4 ± 0.3	-0.2 ± 1.2	1.7 ± 0.1	188.1 ± 44.9	0.4 ± 0.1	40.4 ± 1.1		75.8 ± 0.3	4.4 ± 0.1	-0.6 ± 0.1	4.4 ± 0.1	352.6 ± 0.7	0.2 ± 0.1	6.4 ± 0.2	
Tannic acid	42.5 ± 2.0	29.9 ± 1.3	-5.4 ± 0.5	30.4 ± 1.2	349.7 ± 1.2	2.7 ± 0.4		69.8 ± 3.2	0.3 ± 0.1	3.2 ± 1.4	3.2 ± 1.4	83.5 ± 5.4	0.5 ± 0.1	41.6 ± 0.8		75.7 ± 0.1	2.5 ± 0.1	4.3 ± 0.1	4.9 ± 0.0	420 ± 0.8	0.3 ± 0.1	4.4 ± 0.5	
β-CD	46.2 ± 1.5	28.4 ± 1.7	-5.1 ± 0.9	28.9 ± 1.6	349.8 ± 2.3	2.1 ± 0.2		71.7 ± 3.1	-1.2 ± 0.1	-0.7 ± 0.9	1.5 ± 0.3	294.9 ± 92.1	0.4 ± 0.1	40.2 ± 1.3		76 ± 0.1	4.1 ± 0.1	-0.4 ± 0.1	4.1 ± 0.1	353.9 ± 0.9	0.2 ± 0.1	5.9 ± 0.2	
Alginate	45.7 ± 1.6	28.4 ± 1.3	-5.1 ± 1.2	28.9 ± 1.1	349.8 ± 2.8	2.2 ± 0.2		71.5 ± 3.3	-1 ± 0.4	-0.5 ± 1.4	1.5 ± 0.3	201.2 ± 61.9	0.4 ± 0.1	40.1 ± 1.5		75.3 ± 0.2	4.2 ± 0.1	-0.5 ± 0.1	4.2 ± 0.1	353.6 ± 0.9	0.2 ± 0.1	5.8 ± 0.3	
Oxalic acid	46.2 ± 1.9	28.5 ± 1.6	-5.1 ± 1.0	29 ± 1.4	349.7 ± 2.4	2.1 ± 0.3		71.8 ± 3.4	-1.5 ± 0.1	-0.8 ± 0.5	1.7 ± 0.2	206.5 ± 16.4	0.4 ± 0.1	40.3 ± 1.1		75.9 ± 0.2	4.3 ± 0.1	-0.9 ± 0.1	4.4 ± 0.1	348.3 ± 0.2	0.2 ± 0.1	6.1 ± 0.4	
Gallic acid	46.9 ± 1.1	27.9 ± 1.8	-6.2 ± 1.1	28.6 ± 1.6	347.4 ± 2.6	2.0 ± 0.1		71.7 ± 2.6	-1.8 ± 0.2	-0.5 ± 1.5	2.1 ± 0.1	192.8 ± 42.9	0.4 ± 0.1	40.0 ± 1.9		75.3 ± 0.2	4.4 ± 0.1	-1 ± 0.1	4.5 ± 0.1	347.5 ± 0.8	0.2 ± 0.1	6.6 ± 0.4	
Caffeic acid	46.4 ± 1.6	28.2 ± 1.8	-5.3 ± 1.2	28.7 ± 1.6	349.3 ± 2.9	2.1 ± 0.2		70.4 ± 2.0	-0.9 ± 0.6	-0.8 ± 0.8	1.2 ± 1.0	214.5 ± 17.9	0.4 ± 0.1	39.0 ± 0.3		73.7 ± 0.3	6.4 ± 0.1	0.3 ± 0.1	6.4 ± 0.0	363 ± 0.5	0.3 ± 0.0	7.2 ± 0.1	
Metamord.																							
$SnCl_2$	44.6 ± 1.0	22.1 ± 0.9	-9.1 ± 0.4	23.9 ± 0.8	350.7 ± 2.5	1.9 ± 0.1		71.9 ± 0.8	-0.8 ± 0.2	0.3 ± 0.7	1.0 ± 0.3	42.1 ± 4.1	0.3 ± 0.0	36.9 ± 1.9		71.7 ± 0.2	8.5 ± 0.0	-4.7 ± 0.1	9.7 ± 0.0	353.7 ± 0.8	0.3 ± 0.0	10.6 ± 0.4	
Alum	45.6 ± 0.8	31.5 ± 0.4	-3.3 ± 0.5	31.7 ± 0.4	337.7 ± 1.3	2.2 ± 0.1		71.2 ± 0.2	-0.8 ± 0.1	1.9 ± 0.7	2.1 ± 0.6	285.1 ± 79.4	0.4 ± 0.0	41.6 ± 0.6		73.5 ± 0.3	5.2 ± 0.1	1.8 ± 0.2	5.5 ± 0.1	330.9 ± 0.3	0.3 ± 0.1	6.5 ± 0.2	
Tannic acid	48.4 ± 0.4	38.3 ± 0.6	-7.6 ± 0.1	39.1 ± 0.6	354 ± 0.9	1.8 ± 0.1		76.5 ± 0.1	-1.1 ± 0.4	4.3 ± 2.2	4.5 ± 2.1	116.2 ± 11.7	0.3 ± 0.0	49.9 ± 0.5		77.6 ± 0.1	2.5 ± 0.1	3.3 ± 0.1	4.2 ± 0.1	19.3 ± 1.9	0.2 ± 0.1	4.3 ± 0.5	
β-CD	45.1 ± 0.3	32.1 ± 0.4	-3.6 ± 0.2	32.3 ± 0.4	353.6 ± 0.9	2.3 ± 0.0		71.8 ± 0.2	-0.5 ± 0.1	1.9 ± 1.0	1.9 ± 0.9	109.7 ± 9.6	0.4 ± 0.0	42.4 ± 0.6		74.2 ± 0.2	5.1 ± 0.1	2.0 ± 0.1	5.4 ± 0.0	24.1 ± 2.3	0.3 ± 0.1	6.1 ± 0.2	
Alginate	45.3 ± 1.0	31.9 ± 0.7	-3.6 ± 0.4	32.1 ± 0.7	348.7 ± 0.2	2.3 ± 0.2		71.6 ± 0.4	-0.6 ± 0.2	1.8 ± 0.5	1.9 ± 0.5	107.3 ± 10.7	0.4 ± 0.0	42.2 ± 0.8		74.1 ± 0.2	5.2 ± 0.0	2.3 ± 0.3	5.7 ± 0.1	52.5 ± 1.0	0.3 ± 0.1	6.4 ± 0.1	
Oxalic acid	45.8 ± 0.6	23.6 ± 0.8	-7.7 ± 0.1	24.8 ± 0.7	353.5 ± 0.5	2.2 ± 0.1		72.9 ± 0.6	-0.9 ± 0.2	2.7 ± 1.1	2.9 ± 1.0	106.5 ± 8.6	0.4 ± 0.0	38.0 ± 1.4		73.3 ± 0.5	3.3 ± 0.1	0.9 ± 0.1	3.4 ± 0.1	21.2 ± 0.7	0.3 ± 0.1	4.7 ± 0.4	
Gallic acid	54.7 ± 0.1	30.1 ± 0.2	-9.3 ± 0.3	31.5 ± 0.2	342.0 ± 0.7	1.0 ± 0.0		71.6 ± 0.3	-0.7 ± 0.2	1.9 ± 0.9	2.0 ± 0.8	110.3 ± 9.6	0.4 ± 0.0	36.9 ± 0.3		74.0 ± 0.3	5.1 ± 0.1	2.0 ± 0.1	5.5 ± 0.1	14.9 ± 1.1	0.3 ± 0.0	6.3 ± 0.4	
Caffeic acid	49.7 ± 0.5	32.3 ± 0.2	-4.8 ± 0.5	32.7 ± 0.1	342.8 ± 0.4	1.6 ± 0.1		67.4 ± 0.6	1.9 ± 0.4	0.7 ± 0.7	2.1 ± 0.7	113.7 ± 12.7	0.5 ± 0.0	35.7 ± 0.5		69.8 ± 0.5	14.1 ± 0.2	3.2 ± 0.3	14.5 ± 0.2	21.4 ± 0.6	0.5 ± 0.1	12.7 ± 0.4	

Table 5
The colorimetric properties (D65/10) and color strength of dyed (pre- and metamordanted, washed) according to ISO105-E01 and subjected by light test ISO105–B02 (uncertainties expressed as standard deviation (n = 3)).

	After Washing ISO105-E01								After light test ISO105-B02							
Premord.	L*	a*	b*	C*	h	K/S	ΔE	Samples	L*	a*	b*	C*	h	K/S	ΔE	Samples
Control	56.6 ± 0.9	13.9 ± 2.3	-5.1 ± 0.1	15.0 ± 2.1	339.5 ± 3.5	1.1 ± 0.1	18.9 ± 3.0		61.9 ± 0.1	14.0 ± 0.1	-3.9 ± 0.0	14.5 ± 0.1	344.4 ± 0.1	0.7 ± 0.0	22.0 ± 1.2	
$SnCl_2$	30.7 ± 0.6	14.3 ± 0.5	-13.1 ± 0.5	19.4 ± 0.6	317.6 ± 1.1	4.9 ± 0.2	9.7 ± 2.3		40.7 ± 0.1	15.0 ± 0.1	-14.3 ± 0.1	20.7 ± 0.1	316.4 ± 0.2	2.5 ± 0.0	14.0 ± 0.7	
Alum	57.8 ± 0.6	12.0 ± 1.1	-5.1 ± 0.1	13.1 ± 1.0	336.9 ± 2.1	1.0 ± 0.0	19.8 ± 0.7		62.4 ± 0.3	13.3 ± 0.1	-3.5 ± 0.0	13.8 ± 0.1	345.3 ± 0.1	0.7 ± 0.0	21.8 ± 1.5	
Tannic acid	51.9 ± 1.0	14.7 ± 1.0	-4.2 ± 0.5	15.3 ± 1.1	344 ± 0.7	1.4 ± 0.1	18.0 ± 2.2		54.7 ± 0.1	21.2 ± 0.1	-6.1 ± 0.1	22.1 ± 0.1	344.1 ± 0.2	1.1 ± 0.0	15.0 ± 1.5	
β-CD	56.6 ± 1.3	12.9 ± 1.6	-5.3 ± 0.2	14 ± 1.4	337.3 ± 3.1	1.1 ± 0.1	18.7 ± 3.0		63.2 ± 0.1	13.5 ± 0.1	-3.5 ± 0.0	13.9 ± 0.1	345.4 ± 0.1	0.7 ± 0.0	22.7 ± 1.6	
Alginate	56.2 ± 1.4	14.0 ± 2.2	-5.0 ± 0.1	14.9 ± 2.1	339.9 ± 3.1	1.1 ± 0.1	17.9 ± 3.2		63.2 ± 0.1	13 ± 0.1	-3.5 ± 0.1	13.5 ± 0.1	344.8 ± 0.2	0.7 ± 0.0	23.4 ± 1.4	
Oxalic acid	56.6 ± 1.0	14.3 ± 1.0	-5.8 ± 0.1	15.5 ± 0.9	338 ± 1.8	1.0 ± 0.1	17.6 ± 2.2		63.1 ± 0.2	13.7 ± 0.1	-3.2 ± 0.0	14.1 ± 0.1	346.9 ± 0.1	0.7 ± 0.0	22.5 ± 1.4	
Gallic acid	57.8 ± 0.9	11.4 ± 1.1	-5.3 ± 0.2	12.6 ± 1.0	334.9 ± 2.5	1.0 ± 0.1	19.8 ± 1.1		60.9 ± 0.2	15.5 ± 0.2	-4.4 ± 0.0	16.1 ± 0.1	344.2 ± 0.1	0.8 ± 0.0	18.8 ± 1.7	
Caffeic acid	56.7 ± 1.0	13.0 ± 0.8	-4.4 ± 0.3	13.8 ± 0.7	341.4 ± 2.3	1.0 ± 0.1	18.4 ± 2.6		60.1 ± 0.2	16.9 ± 0.2	-3.2 ± 0.1	17.2 ± 0.2	349.2 ± 0.1	0.8 ± 0.0	17.9 ± 1.5	
Metamord.																
$SnCl_2$	46.4 ± 3.1	15.0 ± 0.3	-13.5 ± 0.3	20.2 ± 0.5	339.5 ± 3.5	1.7 ± 0.4	9.0 ± 1.1		66.7 ± 0.2	10.2 ± 0.1	-5.7 ± 0.1	11.6 ± 0.0	330.9 ± 0.3	0.4 ± 0.0	25.4 ± 1.1	
Alum	56.2 ± 0.8	17.4 ± 1.4	-6.0 ± 0.5	18.4 ± 1.2	318.1 ± 0.1	1.0 ± 0.1	17.8 ± 2.4		59.1 ± 0.0	17.6 ± 0.1	-3.7 ± 0.0	18.0 ± 0.1	348.1 ± 0.0	0.8 ± 0.0	19.4 ± 0.8	
Tannic acid	56.8 ± 0.1	24.0 ± 0.8	-7.2 ± 0.2	25.0 ± 0.8	340.8 ± 3.0	1.0 ± 0.1	16.7 ± 0.4		56.8 ± 0.1	25.3 ± 0.0	-7.6 ± 0.0	26.4 ± 0.0	343.3 ± 0.0	0.9 ± 0.0	15.5 ± 0.8	
β-CD	55.3 ± 1.1	18.7 ± 1.4	-5.4 ± 0.7	19.5 ± 1.1	343.1 ± 2.0	1.1 ± 0.1	16.9 ± 1.9		61.9 ± 0.1	14.6 ± 0.1	-4.4 ± 0.0	15.2 ± 0.1	343.2 ± 0.1	0.7 ± 0.0	24.2 ± 0.4	
Alginate	53.9 ± 1.5	19.0 ± 1.1	-5.8 ± 0.4	19.9 ± 0.9	343.3 ± 0.9	1.2 ± 0.1	15.7 ± 2.9		63.0 ± 0.1	14.2 ± 0.1	-4.2 ± 0.1	14.8 ± 0.1	343.4 ± 0.2	0.6 ± 0.0	25.0 ± 1.1	
Oxalic acid	54.5 ± 1.3	17.8 ± 0.9	-9.2 ± 0.4	20.1 ± 0.8	343.7 ± 3.2	1.1 ± 0.1	10.5 ± 2.4		66.4 ± 0.2	11.4 ± 0.2	-5.9 ± 0.1	12.9 ± 0.2	332.6 ± 0.1	0.5 ± 0.0	24.0 ± 0.7	
Gallic acid	65.4 ± 0.8	17.6 ± 0.8	-8.3 ± 0.4	19.5 ± 0.7	332.8 ± 1.6	0.5 ± 0.1	16.5 ± 1.3		62.5 ± 0.1	22.3 ± 0.1	-6.9 ± 0.0	23.3 ± 0.1	342.8 ± 0.0	0.6 ± 0.0	11.3 ± 0.2	
Caffeic acid	59.1 ± 0.6	22.0 ± 0.3	-5.7 ± 0.3	22.8 ± 0.2	334.9 ± 1.4	0.8 ± 0.1	14.0 ± 0.6		65.4 ± 0.1	19.7 ± 0.1	0.7 ± 0.1	19.7 ± 0.1	2.1 ± 0.2	0.6 ± 0.0	21.0 ± 0.3	

Table 6
Fastness values of staining and color change (CC) of pre- and metamordanted cotton samples according to ISO105–C06 and ISO105-E01 and light test (ISO105–B02) (CDA: diacetate, CO: cotton, PA: nylon, PES: polyester, PC: polyacryl, WO: wool).

	ISO105–C06							**ISO105-E01**							**ISO105–B02**
Premord.	**CDA**	**CO**	**PA**	**PES**	**PAN**	**WO**	**CC**	**CDA**	**CO**	**PA**	**PES**	**PAN**	**WO**	**CC**	
Control	4/5	4	5	5	5	4	2	3/4	2/3	2/3	3	3	3/4	3	1/2
$SnCl_2$	5	4/5	5	5	5	5	2/3	3/4	3	4	4/5	4	5	4/5	3
Alum	5	4	4/5	5	5	4/5	1/2	3/4	2/3	2	3	3/4	4	2	1/2
Tannic acid	5	4/5	5	5	5	5	2	3/4	2/3	2/3	4	4	3	3	3
β-CD	5	4/5	4/5	5	5	4/5	1/2	4	3	2/3	4	4	3/4	2/3	1/2
Alginate	5	4/5	4/5	5	5	4/5	1/2	4	3	2/3	4	4	3/4	2/3	1/2
Oxalic acid	5	4/5	4/5	5	5	4/5	1/2	4	3	2/3	4	3/4	3/4	2/3	1/2
Gallic acid	5	4/5	4/5	5	5	4/5	1/2	4	3	2/3	4	3/4	3/4	2	2/3
Caffeic acid	5	4/5	4/5	5	5	4/5	1/2	4	3	3	4	3/4	3/4	1/2	2/3
Metamord.															
$SnCl_2$	5	4/5	4/5	5	5	4/5	2	4	2/3	4	3/4	3/4	4/5	4	2
Alum	5	4	4/5	5	5	4/5	2	3/4	2	3	3/4	3	3	3	2
Tannic acid	5	4/5	4/5	5	5	4/5	1	3	1/2	3	3	2	3	3	4
β-CD	5	4/5	5	5	5	4/5	1/2	3/4	1/2	2/3	3	3	3	3	2
Alginate	5	4	4/5	5	5	4/5	1/2-2	3/4	2	2	3	2/3	3	3/4	2
Oxalic acid	4/5	3/4	5	5	5	4/5	1/2	3	2	2/3	3	2/3	2	2/3-3	1
Gallic acid	4/5	3	5	5	5	4/5	1/2	3	1/2	3	3	2	3	2-2/3	4
Caffeic acid	4/5	4	4/5	5	4/5	4/5	2	3	1/2	3	3	2	3	2/3	3

in Wang et al. (2016) [17]. This could be ascribed to the gallic acid moieties within tannic acid, which carry antioxidant properties and act as a copigment. It is generally known that tannins possess UV-protection properties [100]. Furthermore, the type of copigment and pH also play a role within the formation of π-π complexes. Bąkowska et al. (2003) [101] show that several anthocyanin-polyphenol copigment complexes were less prone to degradation by UV-irradiation at pH 2.5 where the flavylium ion is exclusively present in solution.

The other two biomordants did not show any significant differences compared to the control sample in both dyeing procedures. The FT-IR spectra did show more intense peaks for O–H stretch, symmetric C–H stretch, HCH and OCH in-plane bending vibration (1423 cm^{-1}) and in-the-plane CH bending (1368 cm^{-1}), which indicates the effective application within premordanting, but this was less pronounced in metamordanting (Figs. S2B and S3B). However, no increased binding by hydrogen bonds or inclusion of anthocyanins were experimentally noticed from the colorimetric data. The results from the fastness tests did not indicate an improved affinity as well. The lack of inclusion by β-cyclodextrin might be assigned to the preferential uptake of the colorless anthocyanin isomers, also called anti-copigmentation effect. The presence of a tetrahedral carbon atom within the hemiketal and chalcone forms, allows a larger flexibility, which makes adaptation to the cyclodextrin cavity far easier, in comparison to the more rigid planar flavylium cation [102]. From the data analyzed, tannic acid shows promising properties as a biomordant, though still inferior to stannous chloride with exception to light fastness.

3.2.3. Biomordant: ionic bond and π-π interactions

After optimizing the esterification procedure, oxalic acid, gallic acid and caffeic acid and an equal amount of SHP was used to fix these biomordants on cellulose. The first to improve the affinity by ionic bonds, the last two by means of π-π interactions. The IR spectrum of oxalic acid was already described in section 3.1.5, the gallic acid spectrum displays similar peaks to that of tannic acid since tannic acid consists of various polygalloyl glucoses. The main notable peak of caffeic acid is a doublet at 1638 cm^{-1} and 1615 cm^{-1}, which shows the trans and vinyl substitution pattern of the alkene (Figs. S2C and S3C). From Table 4, no major differences were visible compared to the control sample in this three-step premordanting procedure. Meanwhile, within metamordanting, intermolecular interactions were clearly visible during the spectrophotometric measurement of the dye uptake. The maximum absorption wavelengths for oxalic, gallic and caffeic acid are shown at 521 nm, 523 and 519 nm, respectively (Fig. S7). Moreover, the relative dye uptakes of oxalic acid and caffeic acid were at least 15% and 20% higher compared to the control sample, respectively. The oxalic acid sample showed a light purplish tint, similar to stannous chloride. Gallic acid gave cotton a very bright pink color (L*: 54.7) due to copigmentation, which comes along with a smaller color strength value and in Table 5, the sample lost a lot of its color strength after the water wash test. The effect of caffeic acid is more distinct during the ISO105–C06 wash step, at which the cotton showed a darker shade (L*: 67.4), during the reimmersion step where the a* value is three times higher compared to the control sample (L*: 69.8, a* = 14.1 and b*: 3.2 ($F(1,4) = 266$, $p < 0.001$; $F(1,4) = 5881$, $p < 0.001$; $F(1,4) = 432$, $p < 0.001$; respectively)) and during the water wash test where the red color is still very strong (a*: 22.0). This can be indicated from the amount of dye that was taken up ($q_{e,s,rel} \geq 7.1$ mg mv-3-glc equiv (g cotton)$^{-1}$) and smaller wash off by this procedure. The ISO105–C06 fastness values for these compounds were only rated poor for color change for both dyeing procedures. A very minor decrease in color change was visible between oxalic acid and the control sample whereas Wang et al. (2016) [17] obtained an increase of 0.5 till 2 grades with increasing succinic acid concentration, implying effective ionic bonds between the treated cotton and dye. One particular issue arises from the use of this acidic environment (pH < 3), which is necessary to obtain the, most stable isomer of anthocyanins, red flavylium cation. This acidic condition jeopardizes the ester bond formed during the premordanting step through acid-catalyzed hydrolysis, explaining the loss of the ester peak after dyeing (Fig. S2F). The color change for the metamordanted samples withstands the water wash test better than the premordanted samples. The results of the light test showed that oxalic acid could not inhibit the color deterioration, whereas a very good light fastness was observed for gallic acid, especially when dyed by metamordanting (ΔE = 11.3 compared to 18.8 by premordanting). Caffeic acid also showed a good light fastness within pre- and metamordanting as shown in Table 6. Concluding, neither oxalic acid nor both aromatic compounds were capable to improve the affinity of the dye for cellulose via ionic bonds or π-π stacking, respectively. However, the latter was able to prevent light induced degradation of anthocyanins by their antioxidant capabilities to some extent due to copigmentation, which is in fact an exothermic process. In most of those complexes experimentally studied, the negative enthalpy factor favours copigmentation while the entropic factor is also negative. The latter refers to the ordering of two compounds within this process, and therefore, limiting the rotational and translational contributions to entropy [31]. For instance, the copigmentation complex between malvin and caffeic acid resulted in a standard Gibbs Free Energy (ΔG°) of −13.6 kJ mol^{-1} (with ΔH° = −25.6 kJ mol^{-1} and ΔS° = 46.0 J mol^{-1} K^{-1}), which decreases more at elevated temperatures [103].

3.3. Modeling of adsorption

The following section describes the results obtained for modeling of adsorption isotherm systems, which represents the event associated with the mobility of a substance from aqueous environments to a solid material at constant temperature and pH.

3.3.1. Adsorption isotherms

The data obtained from the dilution experiment (section 3.1.4) allows the fitting of isotherm models to study the adsorption mechanism (Fig. 4A–C), the important parameters derived from the different isotherm models are described in Table 7. The Langmuir separation factor R_L ($= 1/(1+K_L C_0)$) is 0.97, which means adsorption is favourable. The Freundlich heterogeneity factor *n* shows a slightly higher value than one, indicating a linear adsorption. The two three-parameter models yield similar results for their corresponding isotherm parameters. The X^2 values were lower compared to Langmuir and Freundlich isotherms, providing the best fit to the experimental data. However, the standard deviations for two Redlich-Peterson's variables, a_R and β, were too large for correct interpretation, while the Sips model yields smaller standard deviations and thus, representing the best isotherm model for these data. The exponential parameter n_s, also indicates that the Sips model reduces to the Langmuir model. The solid solute adsorption isotherms can also be classified into different classes: S, L, H and C curves. This classification is useful for interpreting the adsorption mechanism and solute orientation, identifying any impurities or associated solute within the solution and measuring the specific surface area of a solid [104]. From Fig. 4C and D, the $q_{e,s,rel}$ vs C_e plot resembles the C curve with a less steep slope visible after the inflection point. The C curve is characterized by a constant partition of solute between the dyebath solution and the cellulose substrate. The derived parameter K_s represents the partition coefficient and this low value obtained results in a negative log P (−1.3), indicating the hydrophilicity of this dye molecule, which was evidenced by the ISO105-E01 wash test. Bhat et al. (2002) [105] calculated log P values of 86 arylamine dyes from the color index (CI) and found a distribution where 75% of these dyes attained values between 3 and 6 and 35% were above 5, illustrating the more hydrophobic character of synthetic dyes.

3.3.2. Adsorption kinetics

In order to study the adsorption kinetics of mv-3-glc, mathematical models were fitted to the experimental data from the dyeing time (section 3.1.2) to find the most optimal correlation between the adsorbed

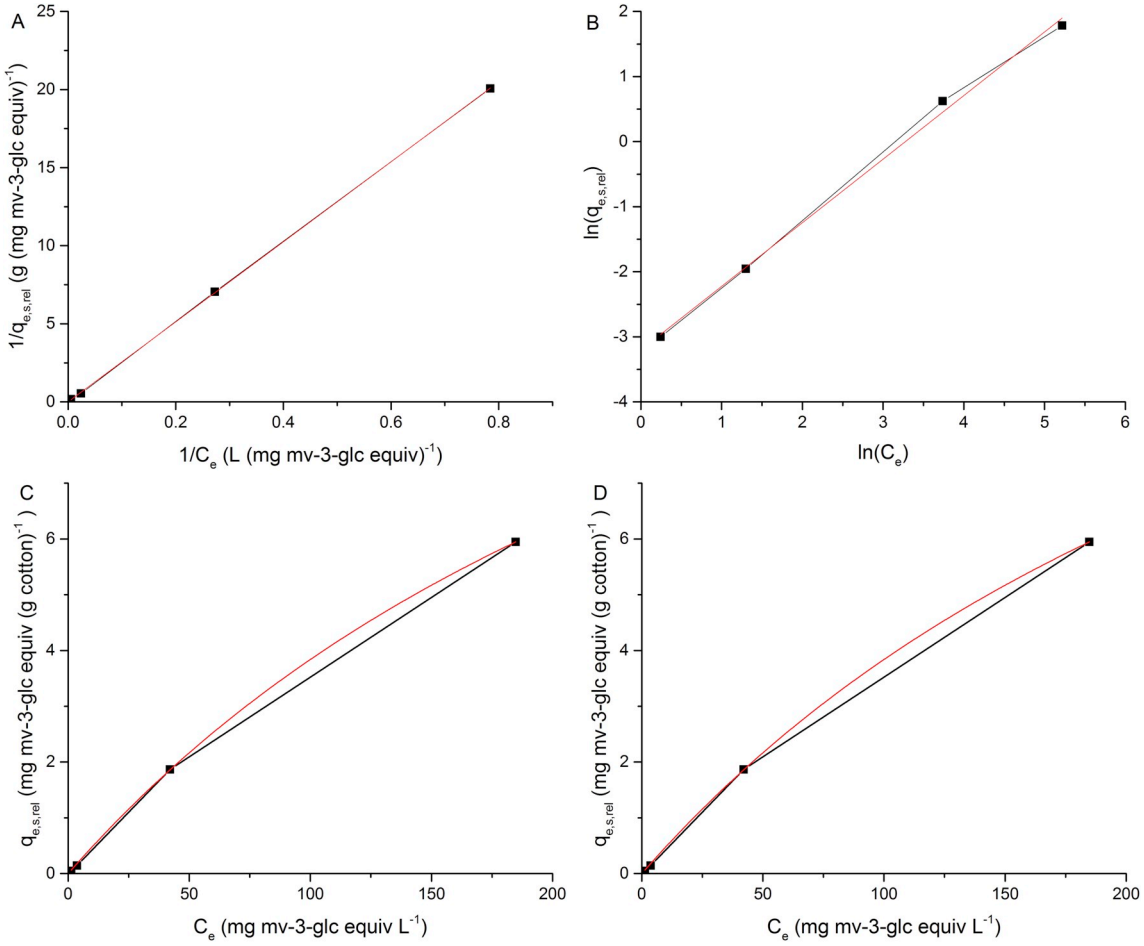

Fig. 4. The isotherm models: Langmuir (A), Freundlich (B), Redlich-Peterson (C) and Sips (D).

Table 7
The isotherm parameters for the adsorption of mv-3-glc on cotton at 80 °C.

Two-parameter model	Parameters	Value	Three-parameter model	Parameters	Value
Langmuir	Q_L (mg g^{-1})	735.29	Redlich-Peterson	a_R (L $mg^{-1})^{\beta}$	0.0029 ± 0.020
	K_L (L g^{-1})	0.000053		β	1 ± 1.14
	R_L	0.97		K_R (L g^{-1})	0.050 ± 0.013
	R^2	0.99996		R^2	0.99993
	X^2	0.22		X^2	0.012
Freundlich	K_F ($mg^{1-1/n}$ $L^{1/n}$ g^{-1})	0.041	Sips	a_S (L $mg^{-1})^{ns}$	0.0029 ± 0.00029
	n_F	1.02		K_S (L g^{-1})	0.050 ± 0.016
	R^2	0.99699		n_s	1.0 ± 0.10
	X^2	0.14		R^2	0.99993
				X^2	0.012

Table 8
The results for the parameters acquired from the adsorption kinetic models.

	Lagergren	Pseudo-second order
q_e (mg mv-3-glc (g cotton)$^{-1}$)	3.64	8.48
k ([a]: min^{-1}, [b]: g (mg min)$^{-1}$)	0.017[a]	0.0010[b]
h (mg (g min)$^{-1}$)	–	0.074
R^2	0.996	0.95
X^2	0.018	0.46
Intraparticle diffusion model		
	Part1	Part2	Part3
k (mg g^{-1} $min^{-1/2}$)	0.19	0.74	−0.0048
C (mg g^{-1})	1.73	−0.39	5.5
R^2	1	0.997	0.0016
X^2	0	0.0016	0.010

amounts of dye and time. The equations used were Lagergren, pseudo-second order and intraparticle diffusion (Table 1). Table 8 describes the results for the adsorption kinetic models applied for the adsorption of mv-3-glc at optimized conditions on cotton. The calculated equilibrium adsorption capacities from both models are also slightly deviated from the real value ($q_{e,s,rel}$ = 6.1 ± 0.2 mg mv-3-glc (g cotton)$^{-1}$) as no appropriate correlation coefficients can be attained with the complete dataset. The intraparticle diffusion model can be depicted by plotting q_t as a function of $t^{1/2}$, which yields a multilinear plot referring to the three-stage process of this model. As displayed in Fig. 5C, the first part of the plot displays the mass transfer of the dye through the solution towards the external surface of the adsorbent, also called boundary layer diffusion. The last two parts could be described as intraparticle diffusion for which the last part is accounted to the final equilibrium stage. The slope of each linear part describes the rate of adsorption. It could be seen that the second part of adsorption is the fastest, which refers to the intraparticle diffusion of the dye through macro- and mesopores, while the third part displays the lowest slope and is related to the diffusion into the micropores of the substrate. The latter is in this case also the rate-limiting step. From the adsorption modeling of anthocyanins on cotton, it can be concluded that this dyeing procedure is a pore size

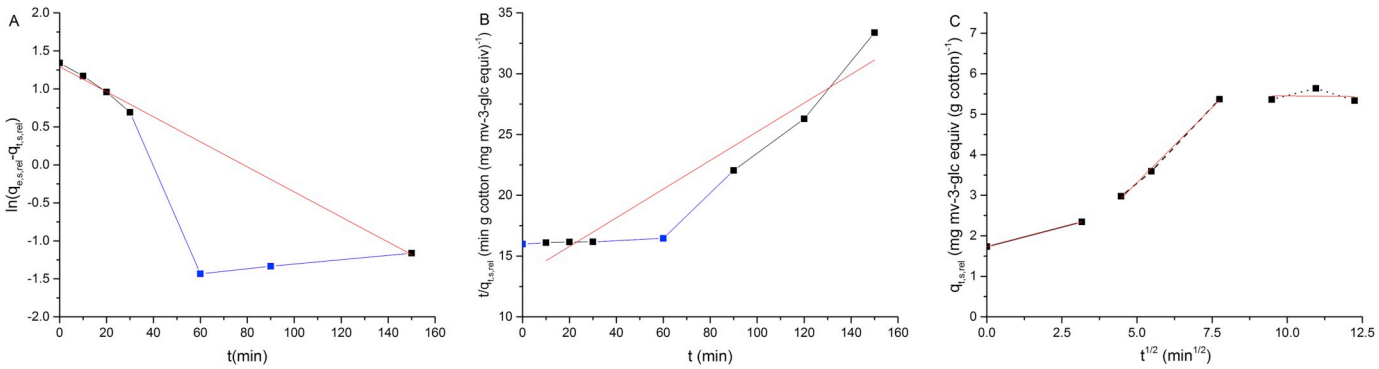

Fig. 5. The kinetic models with from left to right: Lagergren (A), pseudo-second order (B) and intraparticle diffusion model (C). The blue data points were considered as outliers during fitting. (For interpretation of the references to color in this figure legend, the reader is referred to the Web version of this article.)

dependent diffusion process. The pore size distribution for cotton fabrics showed that majority of pores around 50 nm radius is present within cotton fabrics [106] and thus, explaining the higher adsorption rate in the second part of this model. The rate constants in this study are within the same order of magnitude as the study of Cheung et al. (2007) [107] on the adsorption of acid dyes onto chitosan, which also followed a pore size dependent mechanism.

3.4. Molecular modeling of dye-mordants interaction

3.4.1. Interaction energies from static calculations

In this section static DFT calculations are performed to obtain insight into the strength of the intermolecular interactions between dye and mordant and to further explain the experimental observations. As mentioned earlier, it has been studied that stannous chloride, $Sn(II)Cl_2$, oxidizes to the +IV state in acidic environment [72], while diorganotin $(IV)^{2+}$ compounds preferably forms octahedral complexes with flavonoids containing vicinal hydroxyl moieties [75]. Consequently, the tin(IV) coordination complexes were built as octahedral complexes with the chlorine atoms positioned in the trans configuration and two bidentate anthocyanins, as anionic quinoidal bases optimized in section S2.1.1, arranged within the same plane (Fig. 6A). The aluminium salt was modelled as a metal-aquo complex, i.e. an Al(III) cation surrounded by six water molecules in an octahedral fashion whereby the bidentate anthocyanin ligand gradually substitutes two water molecules [34,108]. For cy-3-glc, this yields the following complexes: $[Al(cy\text{-}3\text{-}glc)(H_2O)_4]^{2+}$, $[Al(cy\text{-}3\text{-}glc)_2(H_2O)_2]^{+}$ and $Al(cy\text{-}3\text{-}glc)_3$ (Fig. 6B–D). The Gibbs free energies of the coordination complexes, displayed in Table 9, reveal that tin is able to form the most stable complex with the dye molecules. There were no significant differences visible between the three types of anthocyanins (cy-3-glc, dp-3-glc and pt-3-glc), thus, preferential complexation could be excluded. The aluminium coordination complexes also form stable complexes, which is indicated by the negative Gibbs free complexation energy. Estévez et al. (2011) [34]

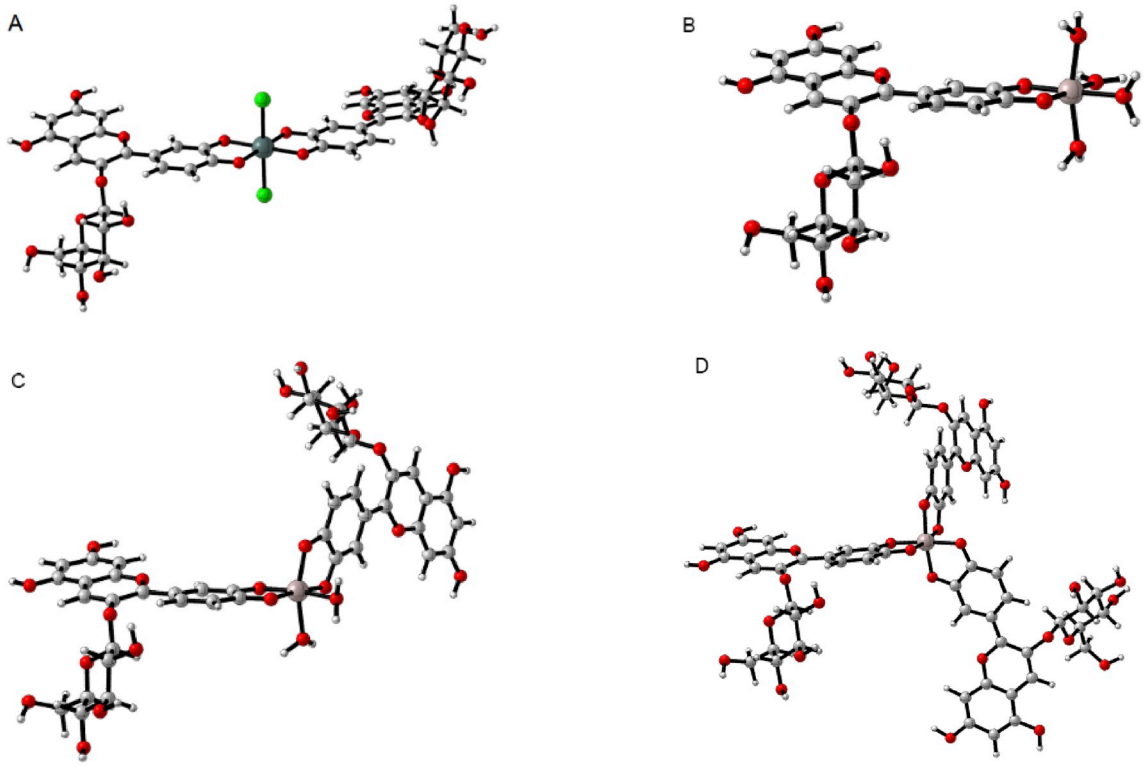

Fig. 6. The 3D illustrations of tin and aluminium coordination complexes with cyanidin-3-glucoside: $Sn(cy\text{-}3\text{-}glc)_2Cl_2$ (A), $[Al(cy\text{-}3\text{-}glc)(H_2O)_4]^{2+}$ (B), $[Al(cy\text{-}3\text{-}glc)_2(H_2O)_2]^{+}$ (C) and $Al(cy\text{-}3\text{-}glc)_3$ (D) (B3LYP/DEF2TZVPP with PCM (water) and Grimme dispersion).

Table 9
The calculated counterpoise (CP) corrected complexation Gibbs free energy values (kJ mol^{-1}) of tin (Sn) and aluminium (Al) coordination complexes with the anthocyanin bidentate ligand.

Conformation	CP corrected $\Delta G_{complex}$ (kJ mol^{-1})[a]	BSSE (kJ mol^{-1})	Type of interactions	Figures
Static calculations				
Metal-ligand complexation[b]				
$Sn(cy\text{-}3\text{-}glc)_2Cl_2$	−954.45	17.57	A Sn(IV) octahedral complex consisting of two anionic quinoidal base molecules with each attached as a bidentate ligand	Fig. 6A
$Sn(dp\text{-}3\text{-}glc)_2Cl_2$	−951.28	17.48		Fig. S9A
$Sn(pt\text{-}3\text{-}glc)_2Cl_2$	−952.77	17.38		Fig. S10A
$[Al(cy\text{-}3\text{-}glc)(H_2O)_4]^{2+}$	−295.33	29.76	An Al(III) octahedral complex with one anionic quinoidal base molecule and 4 water molecules	Fig. 6B
$[Al(dp\text{-}3\text{-}glc)(H_2O)_4]^{2+}$	−295.92	29.79		Fig. S9B
$[Al(pt\text{-}3\text{-}glc)(H_2O)_4]^{2+}$	−291.58	29.65		Fig. S10B
$[Al(cy\text{-}3\text{-}glc)_2(H_2O)_2]^{+}$	−524.99	26.78	An Al(III) octahedral complex with two anionic quinoidal base molecules and 2 water molecules	Fig. 6C
$[Al(dp\text{-}3\text{-}glc)_2(H_2O)_2]^{+}$	−519.55	26.80		Fig. S9C
$[Al(pt\text{-}3\text{-}glc)_2(H_2O)_2]^{+}$	−516.32	26.61		Fig. S10C
$Al(cy\text{-}3\text{-}glc)_3$	−684.96	23.35	An Al(III) octahedral complex with three anionic quinoidal base molecules	Fig. 6D
$Al(dp\text{-}3\text{-}glc)_3$	−689.80	22.99		Fig. S9D
$Al(pt\text{-}3\text{-}glc)_3$	−675.58	23.08		Fig. S10D
Biomordant[c]				
mv-3-glc & hydrogen oxalate[d]	−17.81	3.89	Dye-H(8) … O(6) (1.58 Å) Dye-H(7) … O(5) (2.17 Å)	Fig. S14A
	2.17	3.35	Dye-H(8) … O(4) (1.70 Å) Dye-H(7) … O(5) (2.07 Å)	Fig. S14B
	−9.33	4.22	Dye-H(12) … O(5) (1.53 Å)	Fig. S14C
	23.10	6.89	Dye-O(18) … H(7) (2.11 Å) Dye-H(34) … O(3) (1.98 Å) Dye-H(14) … O(5) (2.33 Å)	Fig. S14D
	15.09	5.74	Dye-H(53) … O(5) (1.60 Å) Dye-O(57) … H(7) (1.86 Å)	Fig. S14E
	23.37	8.73	Dye-O(15) … H(7) (2.90 Å)	Fig. S14F
	18.82	10.48	Dye-H(26) … O(4) (2.44 Å)	Fig. S14G
	15.17	11.01	Dye-H(32) … O(4) (2.30 Å) Dye-H(32) … O(6) (2.57 Å)	Fig. S14H
	23.88	10.67	Dye-O(24) … H(7) (2.49 Å)	Fig. S14I
Dynamic simulations				
Tannic acid	Qualitative		π-π interactions aromatic moieties Tannic acid aromatic moiety 4 and mv-3-glc A ring Tannic acid aromatic moiety 1 and mv-3-glc B-ring	Fig. 9B

[a] ΔG values at 298.15 K.
[b] B3LYP/DEF2TZVPP with PCM and Grimme dispersion.
[c] B3LYP/6–311++G(d,p) with PCM and Grimme dispersion.
[d] Labels are based on Fig. S11.

obtained greater complexation values for the aluminium complexes with cyanidin, but this might be ascribed to the approximations made within their calculations and lack of corrections for dispersion and BSSE. The same researchers performed a more thorough investigation (including the correction factors described above) with the anionic cyanidin-3, 5-di-O-methyl molecule and multiple metal ions, and found that Co (III), Fe(III), Cr(III), and Al(III) are more favored to form a complex, but the values obtained are still high [35]. In general, the aluminium interaction energies obtained remain smaller compared to the tin complexes ($\Delta G_{Sn\text{-}complex,\ avg} = -952.83$ kJ mol^{-1}). It is also worth mentioning that these Gibbs Free Energies obtained are indicative of nature as more detailed numbers can be obtained when hydration free energies would be included for each ionic compound through explicit solvation. Until now, researchers are able to parametrize hydration energies for neutral molecules, which match the experimental values, though elaboration to ionic compounds is more challenging [109]. In the end, these observations match the experimental findings where stabilizing properties of tin were superior to aluminium (section 3.3.1).

The second mechanism to improve the dye's affinity is the creation of anionic sites on cotton, which could attract the positively charged dye molecule. Succinic acid was applied within literature [17], but due to the high pKa value of succinic acid, oxalic acid was opted within this study. Within experiments, the pH of the dyebath is set as such that oxalic acid is present as hydrogen oxalate, i.e. single negatively charged. Firstly, charge and population analyses were performed on hydrogen oxalate and mv-3-glc with Hirshfeld I and MBIS charges (Table S2 and Fig. S11). According to the resonance structure of the flavylium cation, the positive charge is located on the oxygen of the pyrylium ring (compound A in Fig. S13). However, from the charge analysis, it can be shown that the pyrylium oxygen carries a partial negative charge (−0.20), while both carbon atoms on each side of the oxygen carry a partial positive charge (C_2: 0.3 and C_9: 0.45), which corresponds to the delocalized positive charge throughout the flavylium cation system (see Supporting Information S2.1.3). Consequently, ionic interactions are likely not to occur as described within literature. To prove this concept, nine different initial guess complexes containing hydrogen oxalate and mv-3-glc, in close proximity to each other, were investigated for potential intermolecular interactions, i.e. hydrogen bonding and ionic interactions. Only two conformations resulted into a negative complexation Gibbs Free Energy (Table 9 and Fig. S14). As illustrated in Table S4, this can be ascribed to the large negative entropic contribution as complexation comes with the ordering of two compounds. Hence from these calculations, it was concluded that preferential associations between hydrogen oxalate and mv-3-glc are based on hydrogen bonds instead of ionic bonds. Overall, the interaction between the dye and hydrogen oxalate is relatively weak, confirming the experimental results where the application of this biomordant showed similar properties to the control sample.

3.4.2. Molecular dynamics simulations to unravel interactions between tannic acid, dye molecules and solvent

Molecular dynamics simulations were performed to cope with the large and flexible structure of tannic acid, dye and interactions with the aqueous environment. A first MD simulation was applied on a simulation box wherein three dye molecules were positioned around the biomordant in a way that mutual interactions between the dyes were ruled out. It was noticed that one dye molecule diffused away from the complex. A second MD simulation was set up to investigate the interaction of tannic acid with a single dye molecule. Hydrogen bonds were visible between biomordant and dye. The most occurring state is a hydrogen bond interaction between the carbonyl oxygen of the ester function and the OH group at the C_5 or C_7 position or one of the glucose moiety. The combination of two H-bond interactions described above was also observed during certain portions of the MD simulation (Fig. 9A).

However, in order to more realistically mimic the dyeing experiment, a more complex model was set up where also water was added in the simulation box, together with mv-3-glc and tannic acid. it is interesting to investigate in how far water will compete with mv-3-glc or tannic acid. Therefore, a solvent environment has been created in an explicit manner whereby two solvation layers of water molecules surround tannic acid and mv-3-glc molecule. The resulting H-bond interactions were calculated and expressed as a time average of the MD simulation for which a hydrogen bond was formed between dye or tannic acid with water molecules according to the geometrical criteria of Baker and Hubbard (1984) [110] ($\theta_{H \ldots acceptor} > 120°$ and $r_{H \ldots acceptor} <$ 2.5 Å), while hydrogen bonds between water molecules were excluded. It was observed that the hydroxyl groups of the aromatic moieties of tannic acid were largely forming hydrogen bonds with water molecules. Some of the carbonyl oxygen of the ester functions were also continuously undergoing hydrogen bonds with water, making those sites now unavailable for H-bond interactions with the dye (Fig. 7A). Meanwhile, the C_5 and C_7 hydroxyl groups of the dye were barely forming hydrogen bonds compared to the first MD simulation, this could be attributed to a local hydrophobic effect (Fig. 7B). By visualizing the distance between the two molecules in terms of center of mass as a function of time, it can be seen that the A-ring is continuously covered by an aromatic moiety of tannic acid by a characteristic distance of π-π interactions of 3.5 Å (Fig. 8A) [31]. The same trend was also visible for the B-ring (Fig. 8B), while the C-ring did not show any overlap as the dye is aligned to the aforementioned π-π interactions (Fig. 8C). The simulation also showed that when one aromatic moiety of tannic acid leaves the π-π stacking complex, another aromatic moiety fills in that position. Next to that, tannic acid also displays intramolecular π-π interactions (Fig. 9B). Two optional MD simulations within a water box were performed with two and three dye molecules, but taking the concentration effect into consideration, it is the solvent based MD simulation with one tannic acid molecule and one dye that most closely represents the experimental dyeing conditions for tannic acid (see Supporting Information section S2.2.1). From these solvent based MD simulations, we have demonstrated, in a qualitative manner, that the main intermolecular interactions between tannic acid and mv-3-glc are π-π interactions rather than hydrogen bonds. This is in agreement with studies conducted by Kunsági-Máté et al. (2006, 2007) [111,112], wherein π-π interactions were the main intermolecular interactions between malvidin-3-glucoside and other polyphenolic compounds. In general the number of π-π interactions made between tannic acid and the dye molecule, may be anticipated too low to effectively induce strong interactions as described by experimental studies (section 3.2.3). However, the higher color strength and a* value obtained during pre- and metamordanting, respectively, and the good light fastness tests observed within experiments indicated a potential copigmentation effect, which is hereby confirmed.

4. Conclusions

This study has explored the capabilities of anthocyanins as a natural dye on cellulose-based materials and considered 3 main objectives: to optimize the dyeing procedure with anthocyanins for cotton fibers, to investigate the potential of different types of biomordants, which might be equally or more effective compared to metal mordants and to interpret these experimental results by (molecular) modeling approaches.

First, optimized dyeing conditions were based on finding an optimum between dye uptake, color strength, degradation of the natural dye and wash fastness. Therefore, dyeing cotton with anthocyanins is preferred at 80 °C for 60 min at a pH of 1.47 and a concentration 510.7 ± 9.5 mg malvidin-3-glucoside equivalents L^{-1}. Furthermore, fixation of oxalic acid on cotton through esterification was favored at pH 3.

Second, the use of metallic mordants was only successful for stannous chloride with premordanting, which successfully endured the wash- and light tests. The biomordants of interest did not seem to have the required properties to substitute this metal salt. The pH-sensitivity of anthocyanins could not be prevented by any of the biomordants, although it has been proven that the anthocyanins were still slightly

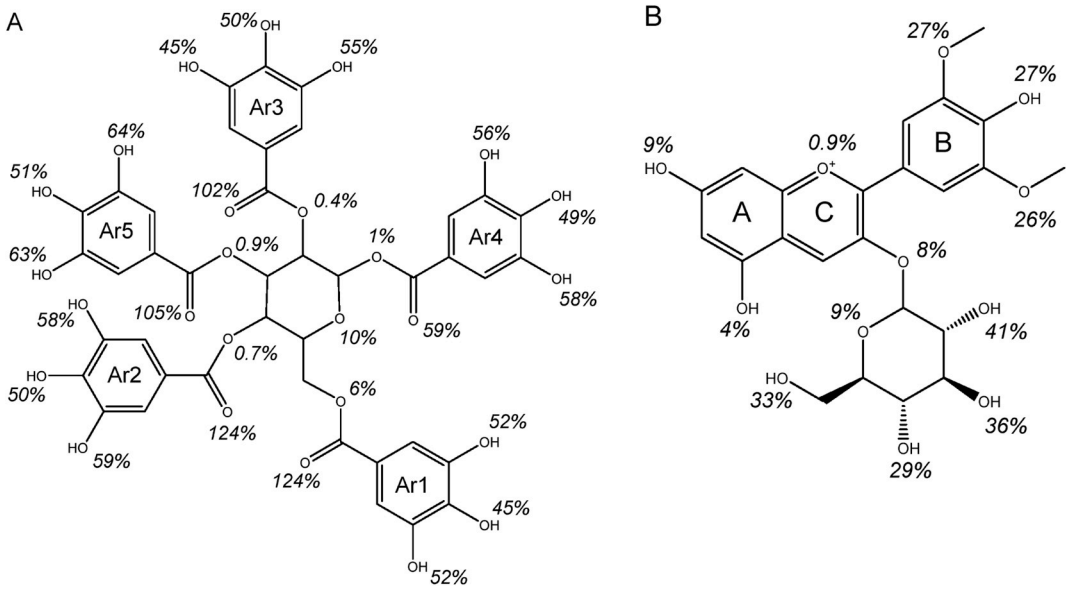

Fig. 7. The time-averaged probability that a functional group of tannic acid (A) and mv-3-glc (B) forms a hydrogen bond interaction.

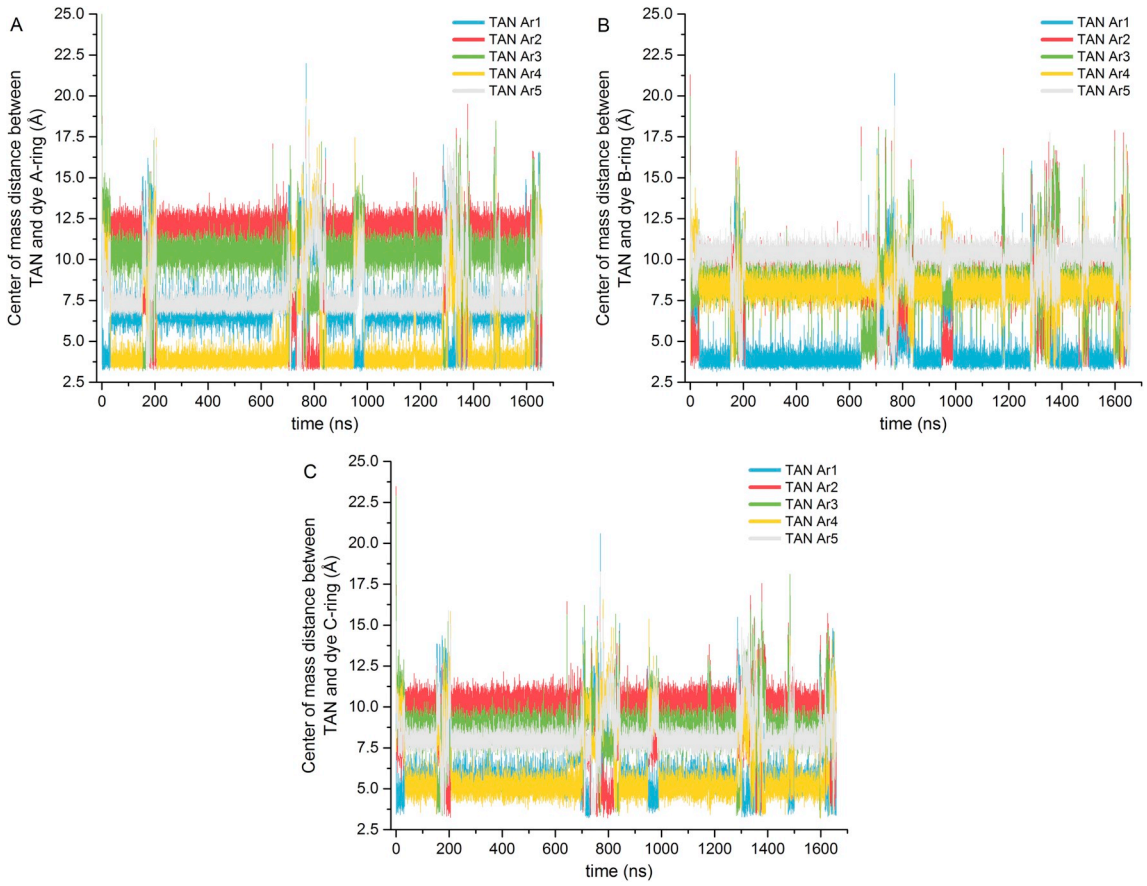

Fig. 8. The visualisation of π-π interactions as interatomic distances between the aromatic groups of tannic acid and the A-ring (A), B-ring (B) or C-ring (C) of mv-3-glc.

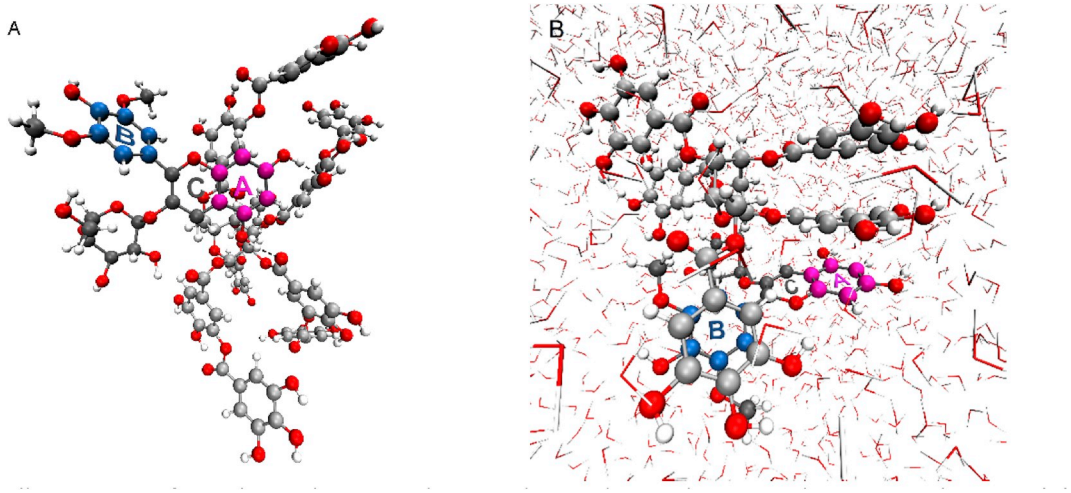

Fig. 9. 3D illustrations of simulation boxes in the gas phase wherein hydrogen bonds are observed (A) and within a water box wherein π-π interactions are highlighted between tannic acid (silver) and mv-3-glc (grey backbone with A-ring: magenta and B-ring: blue) (B). (For interpretation of the references to color in this figure legend, the reader is referred to the Web version of this article.)

present within the fabric when it has been reintroduced within acidic conditions, thus, the main effect is related to the pH of the detergent rather than washing off. This was observed with the wash test of water where a slight to large color loss was visible instead of an alteration. Whereas the biomordants did not show promising results related to the washing tests (ISO150–C06: $\Delta E_{Sn,\ pre} = 26.2$ and $\Delta E_{biomordants,\ pre} \geq 39.0$, ISO105-E01: $\Delta E_{Sn,\ pre} = 9.7$ and $\Delta E_{biomordants,\ pre} \geq 17.6$), the biomordants consisting of phenolic moieties, such as gallic acid and tannic acid, showed their added value in terms of antioxidant property in the light tests (ISO105–B02: $\Delta E_{control} = 22.0$, $\Delta E_{tannic\ acid,\ meta} = 15.5$ and $\Delta E_{gallic\ acid,\ meta} = 11.3$).

Previous findings were corroborated with molecular modeling simulations at different levels of complexity, to obtain insight into strength and type of interactions between the dye and the (bio)mordants. It can

be concluded that the intermolecular interactions, hydrogen bonds and π-π interactions, were too weak in comparison to metal-ligand complexation ($\Delta G_{Sn,avg} = -953$ kJ mol^{-1}, ΔG_{Al} = [-690 kJ mol^{-1}, -282 kJ mol^{-1}]). It was found that anthocyanins are not able to establish ionic bonds with oxalic acid, but only hydrogen bonds ($\Delta G_{hydrogen\ oxalate} = -17.8$ kJ mol^{-1}). Furthermore from the molecular dynamics simulations, it was concluded that the main intermolecular interactions between tannic acid and anthocyanins are governed by π-π interactions and not on hydrogen bonds, which are overall also too weak to yield an efficient dying process.

With this combined experimental and theoretical work, the boundaries of anthocyanins in non-food applications on cotton were established. It is clear that it will be difficult for biomordants to be a real game changer for improving the affinity of natural dyes for textile substrates, despite some 'positive' stories in literature. The stability and affinity of a natural dye initially stands or falls by its molecular structure, notwithstanding analogous "Sn-anthocyanin" complexes can be explored via sustainable building blocks to fit the 'green story'. Currently, applications with anthocyanins can deployed in aqueous environment provided that alkaline substances should be avoided and therefore, are relevant within short life cycle products (e.g. biodegradable products, pH indicator). Future approaches for anthocyanin dyeing could therefore involve enzymatic dyeing or reactive dyeing, by chemical modification. These pathways allow the formation of a covalent bond between dye and substrate, and might potentially be interesting due to the stronger interactions between various components.

Declaration of competing interest

The authors declare that they have no known competing financial interests or personal relationships that could have appeared to influence the work reported in this paper.

CRediT authorship contribution statement

Kim Phan: Conceptualization, Methodology, Writing - original draft, Formal analysis. **Elias Van Den Broeck:** Software, Validation, Writing - review & editing. **Veronique Van Speybroeck:** Conceptualization, Resources, Writing - review & editing. **Karen De Clerck:** Conceptualization, Resources, Writing - review & editing. **Katleen Raes:** Conceptualization, Resources, Writing - review & editing. **Steven De Meester:** Conceptualization, Resources, Writing - review & editing, Supervision, Funding acquisition.

Acknowledgements

The authors would like to thank the Research Board of Ghent University (BOF) for their financial support. The computational resources used in this work were provided by Stevin Supercomputer Infrastructure Ghent University (Belgium) and the Hydra Cluster Vrije Universiteit Brussel (Belgium).

Appendix A. Supplementary data

Supplementary data to this article can be found online at https://doi.org/10.1016/j.dyepig.2019.108180.

References

[1] Saxena S, Raja A. Natural dyes: sources, chemistry, application and sustainability issues. Roadmap to sustainable textiles and clothing. Springer; 2014. p. 37–80.
[2] Kadolph S. Natural dyes: a traditional craft experiencing new attention. Delta Kappa Gamma Bull 2008;75(1).
[3] Mirabella N, Castellani V, Sala S. Current options for the valorization of food manufacturing waste: a review. J Clean Prod 2014;65:28–41. 1016/j.jclepro.2013.10.051.
[4] Rohm H, Brennan C, Turner C, Gunther E, Campbell G, Hernando I, et al. Adding value to fruit processing waste: innovative ways to incorporate fibers from berry pomace in baked and extruded cereal-based foods-A SUSFOOD project. Foods 2015;4(4):690–710. 3390/foods4040690.
[5] Shahid ul I, Mohammad F. Natural colorants in the presence of anchors so-called mordants as promising coloring and antimicrobial agents for textile materials. ACS Sustainable Chem Eng 2015;3(10):2361–75. 1021/acssuschemeng.5b00537.
[6] İşmal ÖE. Greener natural dyeing pathway using a by-product of olive oil; prina and biomordants. Fibers Polym 2017;18(4):773–85. 1007/s12221-017-6675-0.
[7] León-Carmona JR, Galano A, Alvarez-Idaboy JR. Deprotonation routes of anthocyanidins in aqueous solution, pKa values, and speciation under physiological conditions. RSC Adv 2016;6(58):53421–539. 1039/C6RA10818K.
[8] Andersen ØMM KR. Flavonoids : chemistry, biochemistry, and applications. Taylor & Francis Group, LLC; 2006.
[9] Horbowicz M, Kosson R, Grzesiuk A, Dębski H. Anthocyanins of fruits and vegetables - their occurrence, analysis and role in human nutrition. Veg Crops Res Bull. p. 5.
[10] Kahkonen MP, Heinonen M. Antioxidant activity of anthocyanins and their aglycons. J Agric Food Chem 2003;51(3):628–33. 1021/jf025551i.
[11] Castaneda-Ovando A, Pacheco-Hernandez MD, Paez-Hernandez ME, Rodriguez JA, Galan-Vidal CA. Chemical studies of anthocyanins: a review. Food Chem 2009;113(4):859–71. 1016/j.foodchem.2008.09.001.
[12] Francis FJ, Markakis PC. Food colorants: anthocyanins. Crit Rev Food Sci Nutr 1989;28(4):273–314.
[13] Bechtold T, Mahmud-Ali A, Mussak R. Anthocyanin dyes extracted from grape pomace for the purpose of textile dyeing. J Sci Food Agric 2007;87(14):2589–95. 1002/jsfa.3013.
[14] Jung YS, Bae DG. Natural dyeing with black cowpea seed coat. I. Dyeing properties of cotton and silk fabrics. Fibers Polym 2014;15(1):138–44. 1007/s12221-014-0138-7.
[15] Velmurugan P, Kim JI, Kim K, Park JH, Lee KJ, Chang WS, et al. Extraction of natural colorant from purple sweet potato and dyeing of fabrics with silver nanoparticles for augmented antibacterial activity against skin pathogens. J Photochem Photobiol B Biol 2017;173:571–91. 1016/j.jphotobiol.2017.07.001.
[16] Wang H, Hussain M, Zhou W. A novel method for natural dyeing of cotton fabrics with anthocyanin pigments from Morus rubra fruits. Text Res J 2017;87(15):1896–911. 1177/0040517516660887.
[17] Wang H, Tang Z, Zhou W. A method for dyeing cotton fabric with anthocyanin dyes extracted from mulberry (Morus rubra) fruits. Color Technol 2016;132(3):222–31. 1111/cote.12212.
[18] Yasukawa A, Chida A, Kato Y, Kasai M. Dyeing silk and cotton fabrics using natural blackcurrants. Text Res J 2017;87(19):2379–87. 1177/0040517516671125.
[19] Ahmadi Z, Houjeghan FG. Evaluation of color sensitivity to dyeing parameters in natural dyeing with anthocyanin. 2017.
[20] Haddar W, Ben Ticha M, Meksi N, Guesmi A. Application of anthocyanins as natural dye extracted from Brassica oleracea L-var. capitata f. rubra: dyeing studies of wool and silk fibres. Nat Prod Res 2018;32(2):141–81. 1080/14786419.2017.1342080.
[21] Wang CX, Li M, Zhang LP, Fu SH, Wang CX. Extraction of natural dyes from Cinnamomum camphora (L.) presl fruit and their application on wool fabric. Text Res J 2017;87(20):2550–60. 1177/0040517516665266.
[22] Bechtold T, Mussak R, Mahmud-Ali A, Ganglberger E, Geissler S. Extraction of natural dyes for textile dyeing from coloured plant wastes released from the food and beverage industry. J Sci Food Agric 2006;86(2):233–42. 1002/jsfa.2360.
[23] Uddin MG. Effects of different mordants on silk fabric dyed with onion outer skin extracts. J Text. 2014;2014.
[24] Wang H, Li P, Zhou W. Dyeing of silk with anthocyanins dyes extract from liriope platyphylla fruits. J Text 2014;2014. 910.1155/2014/587497.
[25] Yin YJ, Jia JR, Wang T, Wang CX. Optimization of natural anthocyanin efficient extracting from purple sweet potato for silk fabric dyeing. J Clean Prod 2017;149:673–9. 1016/j.jclepro.2017.02.134.
[26] Rose PM, Cantrill V, Benohoud M, Tidder A, Rayner CM, Blackburn RS. Application of anthocyanins from blackcurrant (ribes nigrum L.) fruit waste as renewable hair dyes. J Agric Food Chem 2018;66(26):6790–810. 1021/acs.jafc.8b01044.
[27] Boulton R. The copigmentation of anthocyanins and its role in the color of red wine: a critical review. Am J Enol Vitic 2001;52(2):67–87.
[28] Santos DT, Albarelli JQ, Beppu MM, Meireles MAA. Stabilization of anthocyanin extract from jabuticaba skins by encapsulation using supercritical CO2 as solvent. Food Res Int 2013;50(2):617–24. https://doi.org/10.1016/j.foodres.2011.04.019.
[29] Fernandes A, Rocha MAA, Santos LMNBF, Brás J, Oliveira J, Mateus N, et al. Blackberry anthocyanins: β-Cyclodextrin fortification for thermal and gastrointestinal stabilization. Food Chem 2018;245:426–31. https://doi.org/10.1016/j.foodchem.2017.10.109.
[30] Howard LR, Brownmiller C, Prior RL, Mauromoustakos A. Improved stability of chokeberry juice anthocyanins by β-cyclodextrin addition and refrigeration. J Agric Food Chem 2013;61(3):693–9. 1021/jf3038314.
[31] Trouillas P, Sancho-Garcia JC, De Freitas V, Gierschner J, Otyepka M, Dangles O. Stabilizing and modulating color by copigmentation: insights from review theory and experiment. Chem Rev 2016;116(9):4937–82. 1021/acs.chemrev.5b00507.
[32] Zhao CL, Yu YQ, Chen ZJ, Wen GS, Wei FG, Zheng Q, et al. Stability-increasing effects of anthocyanin glycosyl acylation. Food Chem 2017;214:119–28. 1016/j.foodchem.2016.07.073.
[33] Buran TJ, Sandhu AK, Li Z, Rock CR, Yang WW, Gu L. Adsorption/desorption characteristics and separation of anthocyanins and polyphenols from blueberries

using macroporous adsorbent resins. J Food Eng 2014;128:167–73. https://doi.org/10.1016/j.jfoodeng.2013.12.029.
[34] Estévez L, Otero N, Mosquera RA. Molecular structure of cyanidin metal complexes: Al(III) versus Mg(II). Theor Chem Acc 2011;128(4):485–95. 1007/s00214-010-0829-0.
[35] Estévez L, Sánchez-Lozano M, Mosquera RA. Complexation of common metal cations by cyanins: binding affinity and molecular structure. Int J Quantum Chem 2019;119(6):e25834.
[36] Kunsági-Máté S, Ortmann E, Kollár L, Szabó K, Nikfardjam MP. Effect of ferrous and ferric ions on copigmentation in model solutions. J Mol Struct 2008;891(1). https://doi.org/10.1016/j.molstruc.2008.04.036. 471-4.
[37] Estévez L, Mosquera RA. Where is the positive charge of flavylium cations? Chem Phys Lett 2008;451(1):121–6. https://doi.org/10.1016/j.cplett.2007.11.065.
[38] Woodford JN. A DFT investigation of anthocyanidins. Chem Phys Lett 2005;410(4–6):182–7.
[39] Estévez L, Mosquera RA. A density functional theory study on pelargonidin. J Phys Chem A 2007;111(43):11100–9.
[40] Estévez L, Mosquera RA. Molecular structure and antioxidant properties of delphinidin. J Phys Chem A 2008;112(42):10614–23.
[41] Di Meo F, Sancho Garcia JC, Dangles O, Trouillas P. Highlights on anthocyanin pigmentation and copigmentation: a matter of flavonoid π-stacking complexation to Be described by DFT-D. J Chem Theory Comput 2012;8(6):2034–43. 1021/ct300276pp.
[42] Qian B-J, Liu J-H, Zhao S-J, Cai J-X, Jing P. The effects of gallic/ferulic/caffeic acids on colour intensification and anthocyanin stability. Food Chem 2017;228:526–32. https://doi.org/10.1016/j.foodchem.2017.01.120.
[43] Ferreira da Silva P, Lima JC, Freitas AA, Shimizu K, Maçanita AL, Quina FH. Charge-transfer complexation as a general phenomenon in the copigmentation of anthocyanins. J Phys Chem A 2005;109(32). 7329-3810.1021/jp052106s.
[44] Kalt W, McDonald JE, Donner H. Anthocyanins, phenolics, and antioxidant capacity of processed lowbush blueberry products. J Food Sci 2000;65(3). 390-310.1111/j.1365-2621.2000.tb16013.x.
[45] Burkinshaw SM, Kumar N. Polyvinyl alcohol as an aftertreatment: Part 3 direct dyes on cotton. Dyes Pigments 2010;85(3):124–32. https://doi.org/10.1016/j.dyepig.2009.10.014.
[46] Giusti MM, Wrolstad RE. Characterization and measurement of anthocyanins by UV-visible spectroscopy. Curr Protoc Food Anal Chem 2001;0(1):F1.2.1–1.2.13. John Wiley & Sons, Inc.
[47] Skrede G, Wrolstad R, Durst R. Changes in anthocyanins and polyphenolics during juice processing of highbush blueberries (Vaccinium corymbosum L.). J Food Sci 2000;65(2):357–64.
[48] Lee J, Durst RW, Wrolstad RE. Impact of juice processing on blueberry anthocyanins and polyphenolics: comparison of two pretreatments. J Food Sci 2002;67(5):1660–710. 1111/j.1365-2621.2002.tb08701.x.
[49] Giusti MM, Rodriguez-Saona LE, Wrolstad RE. Molar absorptivity and color characteristics of acylated and non-acylated pelargonidin-based anthocyanins. J Agric Food Chem 1999;47(11):4631–710. 1021/jf981271k.
[50] Hong V, Wrolstad RE. Use of HPLC separation/photodiode array detection for characterization of anthocyanins. J Agric Food Chem 1990;38(3):708–15. 1021/jf00093a026.
[51] Sadilova E, Carle R, Stintzing FC. Thermal degradation of anthocyanins and its impact on color and in vitro antioxidant capacity. Mol Nutr Food Res 2007;51(12):1461–71.
[52] Yue X, Xu Z. Changes of anthocyanins, anthocyanidins, and antioxidant activity in bilberry extract during dry heating. J Food Sci 2008;73(6):C494–910. 1111/j.1750-3841.2008.00845.x.
[53] Foo KY, Hameed BH. Insights into the modeling of adsorption isotherm systems. Chem Eng J 2010;156(1):2–10. https://doi.org/10.1016/j.cej.2009.09.013.
[54] Walton KS, Sholl DS. Predicting multicomponent adsorption: 50 years of the ideal adsorbed solution theory. AIChE J 2015;61(9):2757–62. 1002/aic.14878.
[55] Langmuir I. The constitution and fundamental properties of solids and liquids. Part I. Solids. J Am Chem Soc 1916;38(11):2221–95. 1021/ja02268a002.
[56] Freundlich H. Over the adsorption in solution. J Phys Chem 1906;57(385471):1100–7.
[57] Redlich O, Peterson DL. A useful adsorption isotherm. J Phys Chem 1959;63(6):1024.
[58] Sips R. Combined form of Langmuir and Freundlich equations. J Chem Phys 1948;16(429):490–5.
[59] Arshadi M, Amiri MJ, Mousavi S. Kinetic, equilibrium and thermodynamic investigations of Ni(II), Cd(II), Cu(II) and Co(II) adsorption on barley straw ash. Water Resour Ind 2014;6:1–17. https://doi.org/10.1016/j.wri.2014.06.001.
[60] Fierro V, Torné-Fernández V, Montané D, Celzard A. Adsorption of phenol onto activated carbons having different textural and surface properties. Microporous Mesoporous Mater 2008;111(1):276–84. https://doi.org/10.1016/j.micromeso.2007.08.002.
[61] Piergiovanni PR. Adsorption kinetics and isotherms: a safe, simple, and inexpensive experiment for three levels of students. J Chem Educ 2014;91(4).560-510.1021/ed400267j.
[62] Ho Y-S, McKay G. Pseudo-second order model for sorption processes. Process Biochem 1999;34(5):451–65.
[63] Ho YS, McKay G. A comparison of chemisorption kinetic models applied to pollutant removal on various sorbents. Process Saf Environ Prot 1998;76(4):332–40. https://doi.org/10.1205/095758298529696.
[64] Wu F-C, Tseng R-L, Juang R-S. Initial behavior of intraparticle diffusion model used in the description of adsorption kinetics. Chem Eng J 2009;153(1):1–8. https://doi.org/10.1016/j.cej.2009.04.042.
[65] Ho Y-S. Selection of optimum sorption isotherm. Carbon 2004;42(10). https://doi.org/10.1016/j.carbon.2004.03.019. 2115-6.
[66] Frisch MJ, Trucks GW, Schlegel HB, Scuseria GE, Robb MA, Cheeseman JR, et al. Gaussian 16 Rev. B.01. Wallingford, CT2016.
[67] Becke AD. Density-functional thermochemistry. III. The role of exact exchange. J Chem Phys 1993;98(7):5648–52.
[68] Lee C, Yang W, Parr RG. Development of the Colle-Salvetti correlation-energy formula into a functional of the electron density. Phys Rev B 1988;37(2):785–9.1103/PhysRevB.37.785.
[69] Mercero JM, Matxain JM, Lopez X, York DM, Largo A, Eriksson LA, et al. Theoretical methods that help understanding the structure and reactivity of gas phase ions. Int J Mass Spectrom 2005;240(1):37–99. https://doi.org/10.1016/j.ijms.2004.09.018.
[70] Grimme S, Antony J, Ehrlich S, Krieg H. A consistent and accurate ab initio parametrization of density functional dispersion correction (DFT-D) for the 94 elements H-Pu. J Chem Phys 2010;132(15):154104.
[71] DeMeyer T, Hemelsoet K, VanderSchueren L, Pauwels E, DeClerck K, VanSpeybroeck V. Investigating the halochromic properties of azo dyes in an aqueous environment by using a combined experimental and theoretical approach. Chem Eur J 2012;18(26):8120–89. 1002/chem.201103633.
[72] Young SW. Studies on solutions of stannous salts. II. The oxidation of solutions of stannous chloride by means of free oxygen. J Am Chem Soc 1901;23(3):119–47.1021/ja02029a001.
[73] JO Adeyemi, Onwudiwe DC. Organotin(IV) dithiocarbamate complexes: chemistry and biological activity. Molecules 2018;23(10):257110. 3390/molecules23102571.
[74] Pellerito L, Nagy L. Organotin(IV)n+ complexes formed with biologically active ligands: equilibrium and structural studies, and some biological aspects. Coord Chem Rev 2002;224(1):111–50. https://doi.org/10.1016/S0010-8545(01)00399-X.
[75] Nagy L, Mehner H, Christy AA, Sletten E, Edelmann FT, Andersen QM. Preparation and structural studies on organotin(IV) complexes with flavonoids. J Radioanal Nucl Chem 1998;227(1):89–99. 1007/bf02386436.
[76] Holroyd LF, van Mourik T. Stacking of the mutagenic DNA base analog 5-bromouracil. Theor Chem Acc 2013;133(2). 143110.1007/s00214-013-1431-z.
[77] Bultinck P, Ayers PW, Fias S, Tiels K, Van Alsenoy C. Uniqueness and basis set dependence of iterative Hirshfeld charges. Chem Phys Lett 2007;444(1):205–8. https://doi.org/10.1016/j.cplett.2007.07.014.
[78] Verstraelen T, Vandenbrande S, Heidar-Zadeh F, Vanduyfhuys L, Van Speybroeck V, Waroquier M, et al. Minimal basis iterative stockholder: atoms in molecules for force-field development. J Chem Theory Comput 2016;12(8):3894–912.
[79] Van Damme S, Bultinck P, Fias S. Electrostatic potentials from self-consistent Hirshfeld atomic charges. J Chem Theory Comput 2009;5(2):334–40. 1021/ct800394q.
[80] Verstraelen T, Tecmer P, Heidar-Zadeh F, González-Espinoza CE, Chan M, Kim TD, et al. HORTON 2017;2. 1.1.
[81] VandeVondele J, Krack M, Mohamed F, Parrinello M, Chassaing T, Hutter J. Quickstep: fast and accurate density functional calculations using a mixed Gaussian and plane waves approach. Comput Phys Commun 2005;167(2):103–28. https://doi.org/10.1016/j.cpc.2004.12.014.
[82] Kromann JC, Christensen AS, Steinmann C, Korth M, Jensen JH. A third-generation dispersion and third-generation hydrogen bonding corrected PM6 method: PM6-D3H+. PeerJ 2014;2. e449-e10.7717/peerj.449.
[83] Soper AK. The radial distribution functions of water and ice from 220 to 673 K and at pressures up to 400 MPa. Chem Phys 2000;258(2). https://doi.org/10.1016/S0301-0104(00)00179-8. 121-37.
[84] Martínez L, Andrade R, Birgin EG, Martínez JM. PACKMOL: a package for building initial configurations for molecular dynamics simulations. J Comput Chem 2009;30(13):2157–64.
[85] Wang J, Wang W, Kollman PA, Case DA. Automatic atom type and bond type perception in molecular mechanical calculations. J Mol Graph Model 2006;25(2):247–60.
[86] Wang J, Wolf RM, Caldwell JW, Kollman PA, Case DA. Development and testing of a general amber force field. J Comput Chem 2004;25(9):1157–74.
[87] Price DJ, Brooks III CL. A modified TIP3P water potential for simulation with Ewald summation. J Chem Phys 2004;121(20):10096–103.
[88] Florová P, Sklenovský P, Banáš P, Otyepka M. Explicit water models affect the specific solvation and dynamics of unfolded peptides while the conformational behavior and flexibility of folded peptides remain intact. J Chem Theory Comput 2010;6(11):3569–79. 1021/ct1003687.
[89] Eastman P, Swails J, Chodera JD, McGibbon RT, Zhao Y, Beauchamp KA, et al. OpenMM 7: rapid development of high performance algorithms for molecular dynamics. PLoS Comput Biol 2017;13(7). e1005659-e10.1371/journal.pcbi.1005659.
[90] McGibbon Robert T, Beauchamp Kyle A, Harrigan Matthew P, Klein C, Swails Jason M, Hernández Carlos X, et al. MDTraj: a modern open library for the analysis of molecular dynamics trajectories. Biophys J 2015;109(8):1528–32. https://doi.org/10.1016/j.bpj.2015.08.015.
[91] Tribello GA, Bonomi M, Branduardi D, Camilloni C, Bussi G. Plumed 2: new feathers for an old bird. Comput Phys Commun 2014;185(2):604–13. https://doi.org/10.1016/j.cpc.2013.09.018.
[92] Patras A, Brunton NP, O'Donnell C, Tiwari BK. Effect of thermal processing on anthocyanin stability in foods; mechanisms and kinetics of degradation. Trends Food Sci Technol 2010;21(1):3–11. https://doi.org/10.1016/j.tifs.2009.07.004.

[93] Jackman R, Smith J. Anthocyanins and betalains. Natural food colorants. Springer; 1996. p. 244–309.
[94] Mori K, Goto-Yamamoto N, Kitayama M, Hashizume K. Loss of anthocyanins in red-wine grape under high temperature. J Exp Bot 2007;58(8):1935–45. 1093/jxb/erm055.
[95] Sadilova E, Stintzing FC, Carle R. Thermal degradation of acylated and nonacylated anthocyanins. J Food Sci 2006;71(8):C504–1210. 1111/j.1750-3841.2006.00148.x.
[96] Khoo HE, Azlan A, Tang ST, Lim SM. Anthocyanidins and anthocyanins: colored pigments as food, pharmaceutical ingredients, and the potential health benefits. Food Nutr Res 2017;61(1). 1361779-10.1080/16546628.2017.1361779.
[97] Yang CQ. Effect of pH on nonformaldehyde durable press finishing of cotton fabric: FT-IR spectroscopy study:Part II: formation of the anhydride intermediate. Text Res J 1993;63(12):706–11. 1177/004051759306301202.
[98] Yang CQ. FTIR spectroscopy study of ester crosslinking of cotton cellulose catalyzed by sodium hypophosphite. Text Res J 2001;71(3):201–6.
[99] Fan M, Dai D, Huang B. Fourier transform infrared spectroscopy for natural fibres. Fourier transform-materials analysis. IntechOpen; 2012.
[100] Grifoni D, Bacci L, Zipoli G, Albanese L, Sabatini F. The role of natural dyes in the UV protection of fabrics made of vegetable fibres. Dyes Pigments 2011;91(3):279–85. https://doi.org/10.1016/j.dyepig.2011.04.006.
[101] Bąkowska A, Kucharska AZ, Oszmiański J. The effects of heating, UV irradiation, and storage on stability of the anthocyanin–polyphenol copigment complex. Food Chem 2003;81(3):349–55. https://doi.org/10.1016/S0308-8146(02)00429-6.
[102] Dangles O, Saito N, Brouillard R. Anthocyanin intramolecular copigment effect. Phytochemistry 1993;34(1). https://doi.org/10.1016/S0031-9422(00)90792-1. 119-24.
[103] Galland S, Mora N, Abert-Vian M, Rakotomanomana N, Dangles O. Chemical synthesis of hydroxycinnamic acid glucosides and evaluation of their ability to stabilize natural colors via anthocyanin copigmentation. J Agric Food Chem 2007;55(18):7573–9. 1021/jf071205v.
[104] Giles CH, D'Silva AP, Easton IA. A general treatment and classification of the solute adsorption isotherm part. II. Experimental interpretation. J Colloid Interface Sci 1974;47(3):766–78.
[105] Bhat KL, Garg A, Bock CW. Calculated values of the octanol–water partition coefficient and aqueous solubility for aminoazobenzene dyes and related structures. Dyes Pigments 2002;52(2):145–59. https://doi.org/10.1016/S0143-7208(01)00090-0.
[106] Mao Z, Yu H, Wang Y, Zhang L, Zhong Y, Xu H. States of water and pore size distribution of cotton fibers with different moisture ratios. Ind Eng Chem Res 2014;53(21):8927–34.
[107] Cheung WH, Szeto YS, McKay G. Intraparticle diffusion processes during acid dye adsorption onto chitosan. Bioresour Technol 2007;98(15):2897–904. 1016/j.biortech.2006.09.045.
[108] Shiono M, Matsugaki N, Takeda K. Structure of the blue cornflower pigment. Nature 2005;436(7052). 791-10.1038/436791a.
[109] Riquelme M, Lara A, Mobley DL, Verstraelen T, Matamala AR, Vöhringer-Martinez E. Hydration free energies in the FreeSolv database calculated with polarized iterative Hirshfeld charges. J Chem Inf Model 2018;58(9):1779–97. 1021/acs.jcim.8b00180.
[110] Baker EN, Hubbard RE. Hydrogen bonding in globular proteins. Prog Biophys Mol Biol 1984;44(2):97–179. https://doi.org/10.1016/0079-6107(84)90007-5.
[111] Kunsági-Máté S, Szabó K, Nikfardjam MP, Kollár L. Determination of the thermodynamic parameters of the complex formation between malvidin-3-O-glucoside and polyphenols. Copigmentation effect in red wines. J Biochem Biophys Methods 2006;69(1):113–9. https://doi.org/10.1016/j.jbbm.2006.03.014.
[112] Kunsági-Máté S, Ortmann E, Kollár L, Nikfardjam MP. Effect of the solvatation shell exchange on the formation of malvidin- 3-O-Glucoside−Ellagic acid complexes. J Phys Chem B 2007;111(40). 11750-510.1021/jp.0740144.